

*Infrared radiative performance of urban trees: spatial distribution and interspecific comparison among ten species in the UK by in-situ spectroscopy*

Article

Accepted Version

Creative Commons: Attribution-Noncommercial-No Derivative Works 4.0

Deng, J., Pickles, B. J., Smith, S. T. and Shao, L. (2020) Infrared radiative performance of urban trees: spatial distribution and interspecific comparison among ten species in the UK by in-situ spectroscopy. *Building and Environment*, 172. 106682. ISSN 0360-1323 doi: <https://doi.org/10.1016/j.buildenv.2020.106682> Available at <http://centaur.reading.ac.uk/88560/>

It is advisable to refer to the publisher's version if you intend to cite from the work. See [Guidance on citing](#).

To link to this article DOI: <http://dx.doi.org/10.1016/j.buildenv.2020.106682>

Publisher: Elsevier

All outputs in CentAUR are protected by Intellectual Property Rights law, including copyright law. Copyright and IPR is retained by the creators or other copyright holders. Terms and conditions for use of this material are defined in the [End User Agreement](#).

[www.reading.ac.uk/centaur](http://www.reading.ac.uk/centaur)

## **CentAUR**

Central Archive at the University of Reading

Reading's research outputs online

1 *Manuscript for Building and Environment*

2

3 **Infrared radiative performance of urban trees: spatial distribution**  
4 **and interspecific comparison among ten species in the UK by in-situ**  
5 **spectroscopy**

6

7 Jie Deng <sup>a,\*</sup>, Brian J. Pickles <sup>b</sup>, Stefan T. Smith <sup>a</sup>, Li Shao <sup>a</sup>

8

9 <sup>a</sup> School of The Built Environment, University of Reading, Whiteknights, Reading,  
10 Berkshire, RG6 6DF, UK

11 <sup>b</sup> School of Biological Sciences, University of Reading, Harborne Building,  
12 Whiteknights, Reading RG6 6AS, UK.

13

14 \* Corresponding author:

15 E-mail address: j.deng@reading.ac.uk; deng-jie2@163.com (J. Deng)

16

17 **Infrared radiative performance of urban trees: spatial distribution**  
18 **and interspecific comparison among ten species in the UK by in-situ**  
19 **spectroscopy**

20

21 **Abstract**

22 Understanding the ways in which tree species interact with solar radiation has  
23 previously focused on transmission and reflection of sunlight, typically by examining  
24 individual leaves. Here we used a tree crown spectroscopy measurement method to  
25 conduct in-situ tests on the radiative performance of ten commonly planted tree species  
26 in the UK. Tree crown transfectance (comprehensive effect of transmission and  
27 reflection) was examined to determine i), how radiative performance of individual trees  
28 varies spatially within a species, and ii), how infrared radiative performance differs  
29 between tree species. Our results show that tree crown transfectance depends on the  
30 combination of tree crown morphology, local foliage distribution (leaf density, gaps in  
31 crown foliage contour, concave or convex crown shapes), solar altitude and leaf size.  
32 Spatially, the strongest tree crown transfection was found primarily towards sky on the  
33 sunlit side of trees rather than towards the zenith, meaning that infrared transfection  
34 towards surrounding buildings and pedestrians is substantial. For all ten species, the  
35 tree crown transfectance in the frontal sunlit area was linearly correlated with solar  
36 altitude on sunny days. Hence, a solar altitude of 45° was chosen as the benchmark  
37 condition for comparing interspecific differences. Interspecific comparison indicated

38 that interspecific differences in the infrared radiative performance levels were strongly  
39 dependent on leaf size when no obvious gaps or concave shapes were present within  
40 the tree crowns. Our findings provide insights for understanding radiative interactions  
41 between urban trees and surrounding built environment, as well as for tree species  
42 selection in urban heat stress mitigation.

43

44 *Keywords:* Urban trees; Infrared radiative performance; Tree crown spectroscopy; Tree  
45 species; Urban microclimate

47 **List of symbols**

<b>Nomenclature</b>	
$A_{foliage}$	net foliage area of a measuring patch with foliage gaps, $m^2$
$A_{patch}$	total area of a measuring patch in viewing vision of the fiber-optic tip, $m^2$
$A_{void}$	void area of a measuring patch with foliage gaps, $m^2$
$D_{measured}$	sampling distance from the fiber-optic tip to a measuring patch on tree crown contours
$VA$	viewing angle of the spectrometer fiber-optic tip relative to horizontal plane, $^\circ$
$VR$	void ratio of a measuring patch with foliage gaps, –
$\bar{x}_i$	the $i$ -th average component value of the statistical mean spectrum, –
<i>Greek symbols</i>	
$\alpha$	solar altitude, $^\circ$
$\lambda$	wavelength, nm
$\tau R$	transflectance (comprehensive effect of transmission and reflection) of tree crown contour or canopy patch, –
$\tau R_{mean,800-900}$	mean transflectance in the near infrared wavelength range of 800–900 nm, –
$\tau R(\lambda)$	spectral transflectance at wavelength $\lambda$ nm, –
$\tau R_{foliage}$	net transflectance of foliage excluding foliage gaps in a measuring patch, –
$\tau R_{meas\_bgd}$	background noise signal in sampling transflectance spectrum, –
$\sigma_{A,x}$	type A standard error (uncertainty) of a variable $x$ , unit is the same as $x$
<i>Abbreviations</i>	
$IR$	infrared
$LAI$	leaf area index
$PCA$	principal component analysis
$SAz$	solar azimuth (direction)
$SVF$	sky view factor
$UHI$	urban heat island
$VIS$	visible

## 50 **1 Introduction**

51 Heat waves frequently hit many cities throughout the world and record temperatures  
52 are being experienced in many regions in recent years due to the increasing  
53 temperatures associated with greenhouse gas emissions [1][2]. It is documented that  
54 heat waves have remarkably negative influences on the health of urban inhabitants and  
55 contribute significantly to mortality of residents [1][3][4]. Furthermore, anthropogenic  
56 global warming is increasing the frequency, duration and intensity of heat waves [5],  
57 with the urban heat island (UHI) effect intensifying heat stress under extreme hot  
58 climates [6]. In the pursuit of creating benign urban environments to improve human  
59 health and well-being, it is imperative to seek effective solutions or strategies for  
60 mitigating heat waves and adapting to climate change.

61

62 Trees and green spaces enable the provision of better ecosystem services to urban  
63 environments [7]. For example, urban trees help to mitigate heat waves through  
64 radiative shading [8] and evapotranspiration [9], resulting in lowered air temperatures  
65 that help to regulate outdoor thermal comfort [10][11][12]. Gillner *et al.* [13]  
66 demonstrated that street trees played a key role in mitigating effects of heat and drought  
67 at highly sealed urban sites. Numerical simulations have shown that urban green  
68 coverage (trees and grasslands) helped to mitigate human heat stress under different  
69 climates [14][15], and the same point was argued in a systematic review of urban  
70 greening [16]. Spatial configuration of trees (individual trees versus different types of  
71 spacing and/or aggregations) may show significant, but inconsistent results (including

72 both positive and negative effects) of urban heat mitigation in cities with different  
73 climatic conditions [17][18]. Zhou *et al.* [17] presented that percent cover of trees was  
74 more important than their spatial configuration in predicting land surface temperature  
75 in Baltimore, while the opposite was found in Sacramento. Reasonable urban tree  
76 design approaches have a good performance in mitigating daytime and nighttime UHI  
77 effects in urban environments [19][20], and an appropriate combination of vegetation  
78 and urban geometry can help to mitigate the adverse effects of UHI and provide a better  
79 pedestrian thermal comfort [21][22]. More than that, the cooling effects of urban trees  
80 or green roofs through radiative shading and evapotranspiration also contribute to  
81 building energy savings [12][23] [24] [25]. It is clear that urban forests and trees make  
82 important contributions to cities by providing a multitude of benefits [7]. However, tree  
83 species have different physiological responses to heat waves and extreme heat events  
84 [26][27][28], depending on heat stress adaptability and water availability for the tree  
85 species [29], meaning that some trees cope better with high urban temperatures than  
86 others [26][30].

87

88 To understand urban tree cooling effects and physiological responses, researchers have  
89 been focusing on metrics of assessing outdoor thermal comfort (e.g. surface  
90 temperature, mean radiant temperature, physiological equivalent temperature), tree  
91 physiological indices (e.g. leaf or crown temperature, leaf area index, stomatal  
92 conductance, evapotranspiration rate), determinants and quantification of tree cooling  
93 capacity, tree shade effects and so on. Surface temperatures of trees and green spaces



94 are typically 10–20 °C lower than those of sealed ground or built surfaces exposed to  
95 sunlight in summer, leading to a significant reduction of mean radiant temperature  
96 [13][30][31]. Leuzinger *et al.* [30] reported tree crown temperatures of ten common  
97 tree species planted in Central European cities and declared that tree surface  
98 temperatures were circa -1 to +4 °C higher than the ambient temperature. They found  
99 trees in parks were significantly cooler than those surrounded by sealed ground and  
100 small-leaved trees remained cooler than large-leaved trees. Furthermore, surface  
101 temperatures of different tree species varied considerably, and the SVF (sky view factor  
102 – the ratio of the amount of the sky that can be seen from a given point on a surface to  
103 that potentially available, ranging from 0 to 1) value had a significant effect on tree  
104 surface temperatures [18][32]. It is presumed that the mean radiant temperature, which  
105 is linked to global temperature, air temperature and wind speed [19], is closely related  
106 to the urban thermal comfort [22]. Park *et al.* [33] proposed a multilayer mean radiant  
107 temperature model for pedestrians in a street canyon with trees. Physiological  
108 equivalent temperature is also an important assessing index of outdoor thermal comfort  
109 [18][34]. Zölch *et al.* [35] showed that planting trees had the strongest impact with an  
110 average physiological equivalent temperature reduction of 13% compared with existing  
111 vegetation. Zheng *et al.* [31] measured the influence of trees on the outdoor thermal  
112 environment in subtropical areas through field tests of relevant physiological indices  
113 and microclimatic parameters. They found that the widely planted fig tree *Ficus*  
114 *microcarpa* had the best cooling performance among four tree species studied, with the  
115 maximum reduction of physiological equivalent temperature due to the highest leaf area

116 index (LAI).

117

118 As to the determinants of tree cooling effects in terms of tree physiological indices,  
119 Morakinyo *et al.* [36] revealed that LAI was the main driver of tree cooling for outdoor  
120 temperature regulation, followed by trunk height, tree height and crown diameter. LAI  
121 was also highlighted by Armson *et al.* [37] and Rahman *et al.* [38]. Zhang *et al.* [39]  
122 stated that tall trees with a large LAI and canopy diameter should be a priority to  
123 improve the comfort of outdoor environments. Furthermore, different tree species may  
124 differ in microclimate benefits. Sanusi *et al.* [40] declared that the microclimatic  
125 benefits in streets with *Ulmus procera* and *Platanus x acerifolia* trees were significantly  
126 greater than the street with *Eucalyptus scoparia* trees, in terms of air temperature,  
127 relative humidity, solar radiation, mean radiant temperature, wind speed. In assessing a  
128 tree's cooling capacity via transpiration, it is presumed that different tree species have  
129 significant difference in evaporative cooling [24][41][42][43]. For example, as reported  
130 in [44], *Tilia cordata* trees with higher LAI and sap-wood area provided three times  
131 more transpiration than *Robinia pseudoacacia*. Konarska *et al.* [45] observed that night-  
132 time transpiration in all the seven species they studied amounted to 7 and 20 % of  
133 midday transpiration of sunlit and shaded leaves, respectively, in a high latitude city in  
134 Gothenburg, Sweden. There are some other ways of quantifying the cooling effects of  
135 urban trees through transpiration. For instance, Wang *et al.* [46] quantified the cooling  
136 capacity of urban trees as the surface cooling rate (the negative ratio of land surface  
137 temperature changes to fractional tree cover changes). They found that the surface

138 cooling rate was dominated by plant transpiration, up to 1.336 °C per percentage of  
139 fractional tree cover in heat waves in cities of the contiguous United States.  
140 Additionally, tree shade provides a good outdoor thermal comfort for pedestrians and  
141 enables energy savings. Rahman *et al.* [44][47] investigated vertical air temperature  
142 gradients under tree shades during summer days. Tree radiative shading effect was  
143 simulated by Upreti *et al.* [8] in a regional built environment, who predicted the  
144 capacity of urban trees in reducing urban surface and air temperature by about 2–9 °C  
145 and 1–5 °C, respectively. It is argued that shade trees have more prominent energy  
146 saving potential than urban lawns in a desert city [12]. Urban lawns tend to be hugely  
147 wasteful of water resources, so well chosen species of shade trees or xerophytes may  
148 be far more energy efficient than lawns in arid or semi-arid environments [48][49].

149

150 Apart from research into urban tree cooling effect, reasonable tree planting strategies  
151 were widely considered. Reasonable arrangement of spacing and size of street trees was  
152 proven to be beneficial for decreasing pedestrian mean radiant temperature [50].  
153 Different tree planting strategies are available in [39][51][52][53][54][55][56] for  
154 improving outdoor thermal comfort in different scenarios and climates.

155

156 Generally, previous research into the cooling effect of trees in regulating urban  
157 microclimates simplified the physical characterization of radiative performance of trees  
158 [8][39][57][58][59]. Some studies have excluded the radiative shading effect of trees in  
159 urban microclimatic modelling [60][61]. Where foliage albedo values for different tree

160 species have been incorporated in microclimate modelling to illustrate their influences  
161 on thermal environment they are commonly fixed [59], yet the foliage albedo of trees  
162 varies temporally and spatially throughout a day (as presented in sections 4.2.3 and 4.3  
163 of the present study). To better understand the cooling effect and capacity of urban trees,  
164 it is essential to characterise the radiative performance of different tree species from the  
165 perspective of physical characteristics, especially in the near infrared (NIR) region. In  
166 an earlier study, we established a novel methodology of characterising infrared (IR)  
167 radiative performance of urban trees using tree crown spectroscopy [62]. Experimental  
168 tests on *Tilia cordata* (aka small-leaved lime or little-leaf linden), a commonly planted  
169 tree species in the UK and Europe, were carried out to demonstrate the impact factors  
170 of IR radiative performance qualitatively in terms of transfectance at the tree crown  
171 level. However, the way in which IR radiative performance varies spatially across a tree  
172 crown and interspecific differences remain unanswered. Hence, the present study aims  
173 to explore spatial distribution of IR radiative performance across a tree crown, as well  
174 as to ascertain differences of IR radiative performance levels in tree species that are  
175 often planted in the UK. Since the radiative performance of tree species in terms of the  
176 tree crown transfectance varies with solar time throughout a day in a clear sky, as stated  
177 in our previous work [62], the way in which transfectance varies with solar time was  
178 explored as well, helping to make a benchmark for comparing interspecific  
179 performance differences. Ten commonly planted tree species in the UK were chosen  
180 for extensive in-situ tests of tree crown transfectance on sunny days using the  
181 established spectroscopy measurement method, in order to assess interspecific

182 differences of IR radiative performance levels on the same benchmark.

183

## 184 **2 Test site, method and conditions**

### 185 **2.1 Test site and selection of tree species**

186 Given the convenience and accessibility of trees for extensive in-situ tests, the test site  
187 was chosen at the Whiteknights campus, University of Reading (51.44° N, 0.94° W),  
188 UK. The campus covers an area of 123 hectares and features high plant diversity, with  
189 an estimated number of 150 different tree species. Ten commonly planted tree species  
190 in urban spaces throughout the UK were chosen for tests, as shown in Figure 1. Five of  
191 these are native British trees [63]: *Carpinus betulus* (hornbeam), *Acer campestre* (field  
192 maple), *Quercus robur* (English oak), *Tilia platyphyllos* (large-leaved lime), *Betula*  
193 *pendula* (silver birch).

194



195

196 **Figure 1.** Ten tree species selected in field tests, top row left to right: *Sequoiadendron*

197 *giganteum* (giant sequoia), *Carpinus betulus* ('Fastigiata' cultivar, hornbeam), *Acer*  
198 *campestre* (field maple), *Quercus robur* (English oak) and *Platanus x acerifolia*  
199 (London plane); bottom row left to right: *Tilia platyphyllos* (large-leaved lime), *Acer x*  
200 *freemanii* (autumn blaze maple), *Betula pendula* (silver birch), *Acer platanoides*  
201 ('Schwedleri' cultivar, copper Norway maple) and *Aesculus hippocastanum* (horse  
202 chestnut).

203

## 204 **2.2 Test methods, instruments and facilities**

205 We previously established a methodology for characterising IR radiative performance  
206 of urban trees using tree crown spectroscopy [62]. The term tree crown *transflectance*  
207 ( $\tau R$ ) or *transflection*, which represents comprehensive radiative performance of trees  
208 at the crown level, is introduced in contrast to reflectance or transmittance at tree leaf  
209 levels. This is because when an optical sensor (i.e. spectrometer fiber-optic cable) is  
210 positioned at one side of trees to measure the radiative performance of 'a patch of tree  
211 crown surfaces' (abbreviated as 'measuring patch' hereafter), light received by the  
212 spectrometer usually comprises single-reflected, multi-reflected, multi-transmitted and  
213 transmitted-reflected rays through leaves.

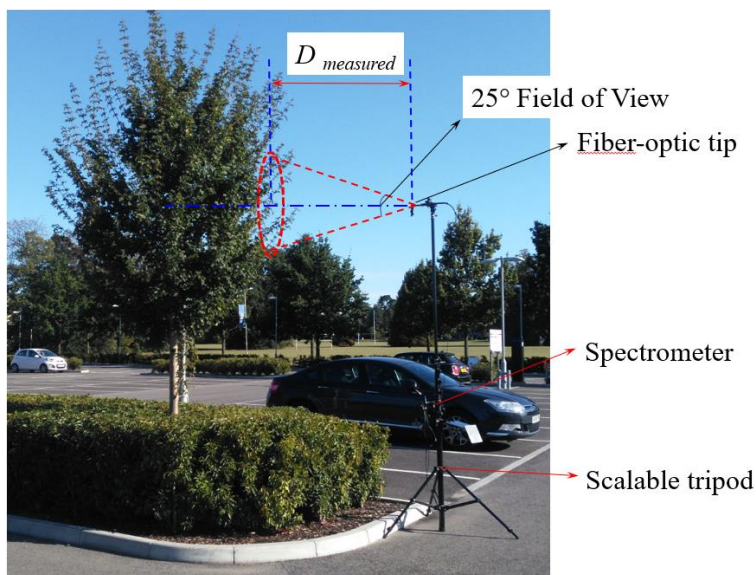
214

215 A Black-Comet-SR model CXR-SR (StellarNET Inc., Tampa, Florida, USA) concave  
216 grating miniature spectrometer with a wavelength range of 350–1000 nm and a  
217 spectroradiometer mode was used for in-situ tests of tree crown transflectance. It covers  
218 the full visible (VIS) region (350–700 nm) and an important spectrum transition from

219 VIS to NIR around 700 nm where the leaf reflectance and crown transreflectance jump  
220 sharply (see testing results in section 4). Its spectral resolution is 0.5 nm. In the  
221 spectroradiometer mode, the fiber-optic tip can be fitted with a cosine receptor which  
222 allows measurement of solar spectra irradiance in a 180° field of view in the 350–1000  
223 nm wavelength range. The spectroradiometer mode was only used for solar spectral  
224 irradiance measurements in conditions of different viewing angles of the fiber-optic tip.  
225  
226 Regarding the test facilities, a scalable tripod with a full height of 8 m was used to hold  
227 and position the fiber-optic cable of the miniature spectrometer in the field tests, as  
228 shown in Figure 2(a). The fiber-optic cable was mounted onto the top of the tripod at  
229 one end and connected to a data acquisition laptop at the other. A USB camera was  
230 fixed close to the fiber-optic tip in order to capture viewing vision of the latter in field  
231 tests. The miniature spectrometer was powered through a USB cable connected to the  
232 laptop. The battery when fully charged usually lasted for about five hours powering  
233 both the laptop and the spectrometer. The viewing angle of the optical sensor can be  
234 adjusted in all directions. The fiber-optic cable was usually used without any cosine  
235 receptor and had a field of view of 25°. A reflectance standard RS50 shown in Figure  
236 2(b) was adopted to measure reference spectra. The reference spectrum was always  
237 sampled in a vertical plane in the transient solar azimuth (SAz) direction, as justified in  
238 our previous work [62]. Particularly, for a test sequence of transreflectance spatial  
239 distribution, a single vertical reference plane was employed, and the test sets were  
240 performed within several minutes. Appropriate measuring distance from the trees  
241 should be chosen to make the measuring results robust. It was found that the sampling

242 distance ( $D_{measured}$  in Figure 2(a)) from the fiber-optic tip to the measuring patches  
243 on the tree crown surfaces could not be too close (e.g. less than 1.5 m), as it would lead  
244 to higher transfectance levels than a sampling distance beyond 2.0 m where the  
245 measuring result was robust. This measurement issue was greatest for tree species with  
246 large-sized leaves such as *Platanus x acerifolia* (London plane), *Aesculus*  
247 *hippocastanum* (horse chestnut), in which the IR transfectance would be overestimated  
248 by 25% at a closer sampling distance (e.g. 1.0 m) due to a specular reflectance effect  
249 from partial leaf surfaces. In view of this, the sampling distance was kept between 2.0–  
250 5.0 m for most of the tested trees, depending on the tree crown diameters and the  
251 viewing vision of the USB camera. In some small trees, e.g. *Acer campestre* (field  
252 maple) a distance of 1.5–2.0 m was chosen because the height of the trees was less than  
253 5 m and the diameter of the tree crowns was less than 3 m.

254



255 (a)





256 (b)

257 **Figure 2.** (a) A scalable tripod holding the optical fiber spectrometer for field tests; (b)  
258 Optic fiber tip of the spectrometer and a reflectance standard RS50.

259

260 A model SM2500 spectrometer (Spectral Evolution, Haverhill, Massachusetts, USA)  
261 with spectral resolution of 3.5–22 nm in the full range of UV (ultraviolet), VIS, NIR  
262 (wavelength range: 350–2500 nm and wavelength reproducibility of 0.1 nm at an  
263 accuracy of 0.5 bandwidth) was used in the laboratory to measure leaf reflectance of  
264 different tree species, in contrast to the tree crown transreflectance levels. The  
265 spectrometer was deployed together with a leaf clamp supplied by the manufacturer for  
266 leaf reflectance measurements. This spectrometer with a broad spectral range was bulky  
267 and expensive, thus not suitable for mounting on a tripod for field tests.

268

### 269 **2.3 Test conditions**

270 To explore spatial distribution rules of the radiative performance of individual trees,  
271 one fastigate hornbeam tree of 7.0 m height and one *Acer campestre* tree of 4.4 m  
272 height were primarily measured at multiple times, with different viewing angles of the  
273 spectrometer fiber-optic tip pointing at different spatial locations of their crowns. Wider  
274 field tests of the ten tree species were implemented to explore interspecific differences

275 of the radiative performance in terms of the transflectance in the sunlit area of trees. At  
276 least five individual trees were sampled for each species in order to assess both  
277 intraspecific (within-species) and interspecific (between-species) variability in  
278 transflectance. All field tests of tree crown transflectance were carried out on sunny  
279 days or in sunny time slots without clouds shading the sun, in order to maintain a  
280 constant solar irradiance for the reference spectrum and the sampling transflectance  
281 spectrum. Measuring heights of the transflectance were usually chosen around the  
282 center height of the tree crown within  $\pm 1.0$  m deviation. Background noise signal was  
283 measured for several individual trees to assess its impact on measurements, which was  
284 found to be negligible as shown in section 4.2.1.

285

286 In addition to meteorological microclimate conditions (outdoor air temperature,  
287 incoming and outgoing shortwave radiation, incoming and outgoing longwave  
288 radiation), the soil moisture contents and physiological conditions (leaf temperature) of  
289 a single fastigate hornbeam (*Carpinus betulus*) tree were monitored during the testing  
290 period of June to September 2019, providing information reference for the test  
291 conditions. Chlorophyll fluorescence and heat stress of five tree species were measured  
292 to inform their physiological stress status. Reflectance spectra of multiple individual  
293 leaves of various tree species were also measured in the lab for contrast.

294

295

### 296 **3 Data processing and error analysis**

297 Repeated measurements of leaf reflectance or tree crown transflectance spectra for

298 various tree species were implemented to obtain the statistical mean. Notate  $M$  as the  
 299 number of spectra samples of a specific tree species. For each spectrum sample, assume  
 300 that  $N$  rows of spectral values are recorded at different wavelength intervals. The  
 301 statistical mean spectrum is calculated based on the sample component values in each  
 302 row, as given in Equation (1).

$$303 \quad \bar{x}_i = \sum_{j=1}^M x_{i,j} \quad (1)$$

304 where  $\bar{x}_i$  is the  $i$ -th average component value of the statistical mean spectrum, while  
 305  $x_{i,j}$  ( $i = 1, 2, 3, \dots, N$ ;  $j = 1, 2, 3, \dots, M$ ) denotes the  $i$ -th measured component value  
 306 in the  $j$ -th sample spectrum.

307

308 With respect to error analysis of the statistical mean spectrum of the tree crown  
 309 transfectance or the reflectance of individual leaves, A-type standard error (uncertainty)  
 310 is usually used to estimate the statistical mean errors [64], as described in Equation (2).

311

$$312 \quad \sigma_{A,x} = \sqrt{\frac{1}{M(M-1)} \sum_{j=1}^M (x_j - \bar{x})^2} \quad (2)$$

313

314 where  $\sigma_{A,x}$  is the A type standard error of a variable  $x$ ,  $M$  is the number of samples,  
 315  $\bar{x}$  is the statistical mean value of variable  $x$ , and  $x_j$  represents the  $j$ -th sample value.

316

317 The standard error of the statistical mean tree crown transfectance or leaf reflectance  
 318 spectrum at each wavelength band is therefore given by:

$$319 \quad \sigma_{A,\tau R}(i) = \sqrt{\frac{1}{M(M-1)} \sum_{j=1}^M (x_{i,j} - \bar{x}_i)^2} \quad (3)$$

320

321 where  $\sigma_{A,\tau R}(i)$  is the  $i$ -th component of the A-type standard error for the transfectance  
322 ( $\tau R$ ) spectrum.

323

324 When calculating the statistical mean, if a spectrum in the samples was found to be  
325 outside of the 99.8% confidence interval, i.e.  $[-3\sigma_{A,TR}, +3\sigma_{A,TR}]$ , it was identified as  
326 a spectrum outlier. The statistical mean of the targeted spectrum was then recalculated  
327 excluding any outliers to minimize the contribution of measurement errors or non-target  
328 biological processes such as damaged or discolored leaves.

329

### 330 **3.1 Statistical analyses using PCA (principal component analysis)**

331 Unless otherwise noted all statistical analyses using PCA were carried out in R version  
332 3.6.0 [65]. Packages “vegan” [66], “factoextra” [67] and “FactoMineR” [68] were used  
333 to analyse spectral data. Due to the nature of this data, ordination using Principal  
334 Component Analysis (PCA) and Principal Coordinates Analysis (PCoA or MDS -  
335 Multidimensional Scaling) generate the same outcome; for consistency these  
336 ordinations are referred to as PCA. Briefly, PCA takes a multivariate dataset of  
337 potentially correlated variables and transforms them into fewer, uncorrelated variables  
338 (principal components). This approach is commonly applied in ecology (see Legendre  
339 and Legendre [69]) and has previously been applied to leaf spectral data in remote  
340 sensing studies (e.g. Cavender-Bares et al. [70]). Spectral data (transfectance measured  
341 across the range 350-1000 nm) were interpolated for each of 67 individual trees from

342 0.5 nm bands into 5 nm bands and then scaled prior to analysis. The 10-fold reduction  
343 in data points following interpolation (1300 to 130 bands per tree) led to a loss of only  
344 0.1% of overall explained variance. Significant correlations between PCA axes and  
345 spectra were used to assess the specific differences represented by the axes, and species  
346 was used as a grouping variable.

347

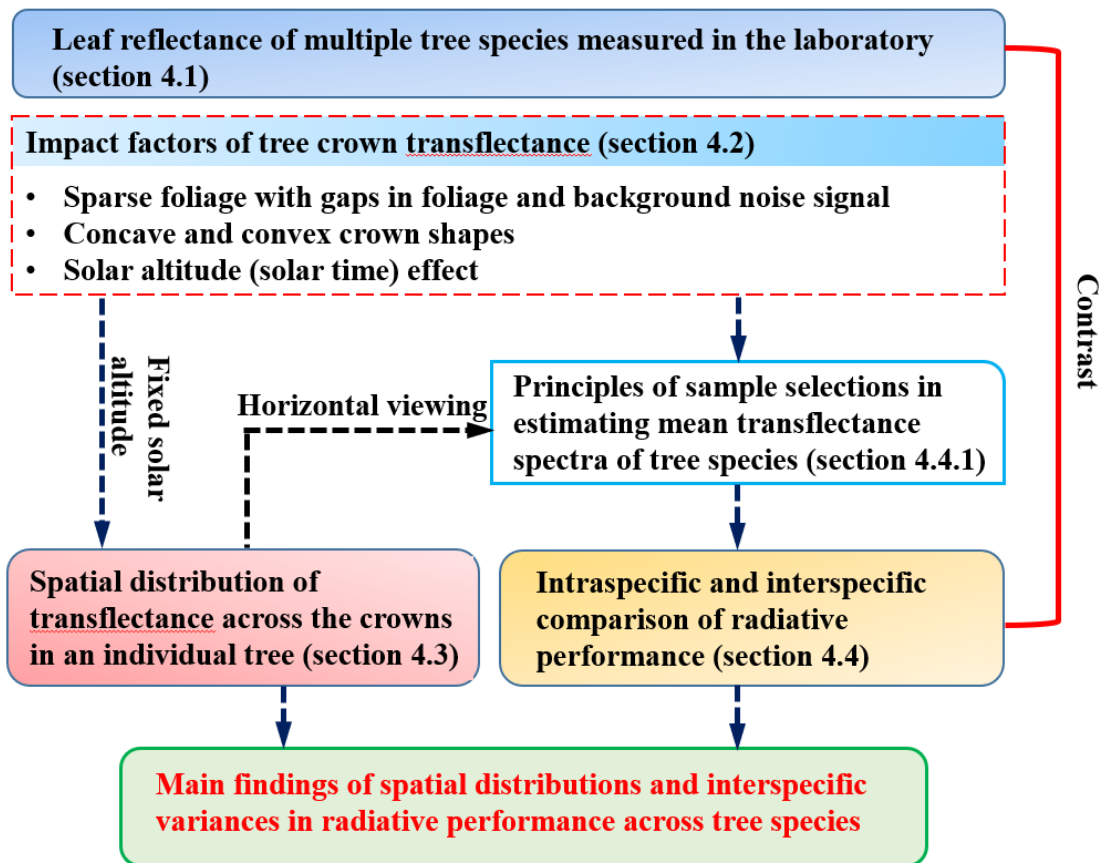
348 Further examination of inter- and intra-specific differences in transmittance profiles for  
349 350-1000 nm was conducted by converting PCA eigenvalues into pairwise euclidean  
350 distances and then applying permutational multivariate analysis of variance  
351 (PERMANOVA) on the resulting distance matrices. The multivariate homogeneity of  
352 dispersion (variance) was then assessed to examine the extent to which observed  
353 differences i) could be attributed to interspecific differences in transmittance values, or  
354 ii) may have been confounded by differences in intraspecific variance.

355

#### 356 **4 Results and discussion**

357 Figure 3 illustrate the flow chart of research framework in the discussion, in order to  
358 determine i), how radiative performance of individual trees varies spatially within a  
359 species, and ii), how infrared radiative performance differs between tree species.

360



361

362 **Figure 3.** Flow chart of the research framework in discussion.

363

#### 364 4.1 Leaf reflectance measured in the laboratory

365 Leaf reflectance spectra of 9 targeted tree species (except *Sequoiadendron giganteum*)

366 were measured at multiple times in the laboratory using the SM2500 spectrometer

367 (Spectral Evolution) with a leaf clamp, in order to estimate statistical mean leaf

368 reflectance spectra. Leaf reflectance of the species *Sequoiadendron giganteum* was not

369 measured, as the spectrometer could not be used to measure individual needle leaves.

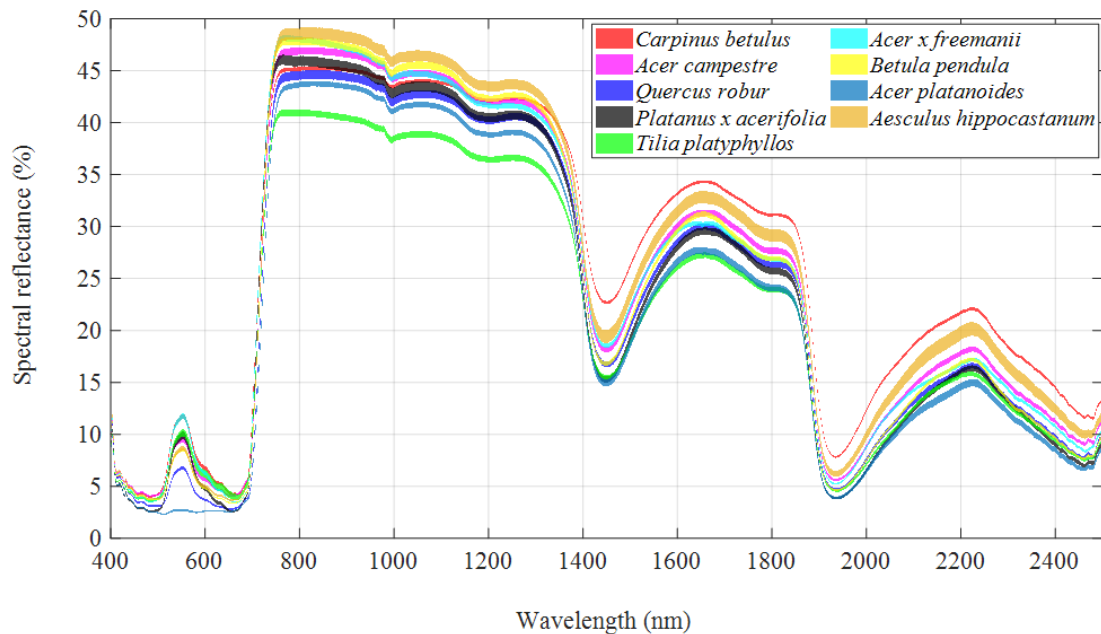
370 For each tree species, 10 leaves were collected randomly from individual trees and 5–

371 10 trees were sampled. Reflectance spectra of the collected leaves were measured

372 within 1 hour after leaf collections to guarantee that the leaves would not lose moisture.

373 Each selected leaf was measured once, and the measuring point was chosen randomly  
 374 with consideration of avoiding main leaf veins. Figure 4 gives the statistical mean leaf  
 375 reflectance spectra of 9 tree species, indicating there is a minor difference of mean leaf  
 376 reflectance spectra among various tree species (within  $\pm 4\%$  of spectral reflectance  
 377 values). The standard mean errors of spectral reflectance of various tree species in the  
 378 wavelength range of 400–2500 nm were within  $\pm 0.5\%$  with a large number of samples  
 379 (50–100 samples for each species). Data on statistical mean reflectance spectra of  
 380 leaves across species can be accessed in *Appendix A*.

381



382

383 **Figure 4.** Standard mean error bands of leaf reflectance spectra of nine tree species  
 384 measured in the laboratory and sampled from 5–10 trees for each species.

385

#### 386 **4.2 Impact factors of tree crown transreflectance**

387 Through a multitude of in-situ tests, it was found that visibly non-uniform foliage

388 distribution in the measuring patches of tree crown contours, such as sparse foliage with  
389 gaps in crown foliage and/or concave crown shapes, would affect tree crown  
390 transfectance ( $\tau R$ ) to different extents. On the other aspect, our previous work  
391 indicated that solar time was one of the most important factors impacting  $\tau R$  levels  
392 [62]. It is therefore necessary to elucidate the impacts and determine the principles of  
393 sample selections for estimating the radiative performance levels of multiple tree  
394 species.

395

#### 396 **4.2.1 Impact of sparse foliage with gaps in crown foliage and background noise** 397 **signal**

398 Sparse foliage is commonly visible at some locations of tree crowns. To estimate  
399 measurement errors of the measuring patches with gaps in the sparse foliage and  
400 examine the impact of background noise signal penetrating the gaps, it is essential to  
401 measure the transfectance of the measuring patch along with the background noise  
402 signal. Void ratio of the gaps in the measuring patch should be also determined, in order  
403 to correct the net transfectance of the sparse foliage by excluding background noise  
404 signal. Total area of a measuring patch with gaps ( $A_{patch}$ ) is sum of the net foliage area  
405 ( $A_{foliage}$ ) and the void area ( $A_{void}$ ) in equation (5). Void ratio of the gaps ( $VR$ ) is  
406 calculated in equation (6). Relation between the measured transfectance  
407 ( $\tau R_{meas\_patch}$ ), the net transfectance of foliage ( $\tau R_{foliage}$ ) and the background noise  
408 signal ( $\tau R_{meas\_bgd}$ ) is described by equation (7) based on radiative energy conservation.  
409 Thus, the net transfectance of foliage ( $\tau R_{foliage}$ ) is rearranged in equation (8) and the  
410 relative error is estimated by equation (9).



$$411 \quad A_{patch} = A_{foliage} + A_{void} \quad (5)$$

$$412 \quad VR = A_{void}/A_{patch} = A_{void}/(A_{foliage} + A_{void}) \quad (6)$$

$$413 \quad \tau R_{meas\_patch} = \frac{\tau R_{foliage} \cdot IRR_{ref} \cdot A_{foliage} + \tau R_{meas\_bgd} \cdot IRR_{ref} \cdot A_{void}}{A_{patch} \cdot IRR_{ref}}$$

$$414 \quad = \tau R_{foliage} \cdot VR + \tau R_{meas\_bgd} \cdot (1 - VR) \quad (7)$$

$$415 \quad \tau R_{foliage} = \tau R_{meas\_patch} + \frac{VR}{1 - VR} \cdot (\tau R_{meas\_patch} - \tau R_{meas\_bgd}) \quad (8)$$

$$416 \quad Error_{sparsefoliage} = \frac{VR}{1 - VR} \cdot \left(1 - \frac{\tau R_{meas\_bgd}}{\tau R_{meas\_patch}}\right) \times 100\% \quad (9)$$

417

418 Take the  $\tau R$  measurement of a *Tilia platyphyllos* tree with sparse foliage as an example  
 419 to illustrate the impact of background noise. Figure 5(a) shows the viewing vision of  
 420 the tree crown  $\tau R$  measurement in the sunlit area and SAz (solar azimuth) direction  
 421 with solar altitude  $\alpha = 34^\circ$ . The void ratio of gaps (VR) in the vision was estimated by  
 422 the ImageJ software [71], resulting in  $VR = 23.3\%$  (see Figure 5(b)). The net  $\tau R$  of  
 423 the foliage ( $\tau R_{foliage}$ ) was calculated in equation (8). Figure 5(c) shows the corrected  
 424 net foliage  $\tau R$  spectrum excluding gaps in foliage compared to the measured  $\tau R$   
 425 spectra. It suggested that the measurement error by the background noise was very  
 426 small (within 3% deviation). Furthermore, the net  $\tau R$  of the foliage was lower (-4%  
 427 deviation of IR  $\tau R$  in this case) than the  $\tau R$  of a dense measuring patch in another  
 428 *Tilia platyphyllos* tree, indicating that a sparse foliage (sparse leaf density) degraded the  
 429  $\tau R$  levels.

430

431 Distributions of sparse foliage on individual trees are amorphous and heterogeneous,  
 432 resulting in different values of void ratio. When choosing measuring patches with

433 visibly dense foliage (no obvious gaps,  $VR < 10\%$ ), it is easy to control the measuring  
434 errors. For most of the trees in tests,  $VR \approx 5\%$ , while the observed spectral  
435 transfectance between the measuring patches and the background noise signal is  
436 usually less than 30% ( $\tau R_{meas\_patch} - \tau R_{meas\_bgd} \leq 30\%$ ), it implies that the absolute  
437 measurement error of the transfectance is below 3% using equation (9). In this sense,  
438 background noise in the transfectance measurement with visibly dense foliage can be  
439 disregarded.

440



441

442 (a) Viewing vision (circle in red dashed line) of the tree crown transfectance  
443 measurement in the SAz direction



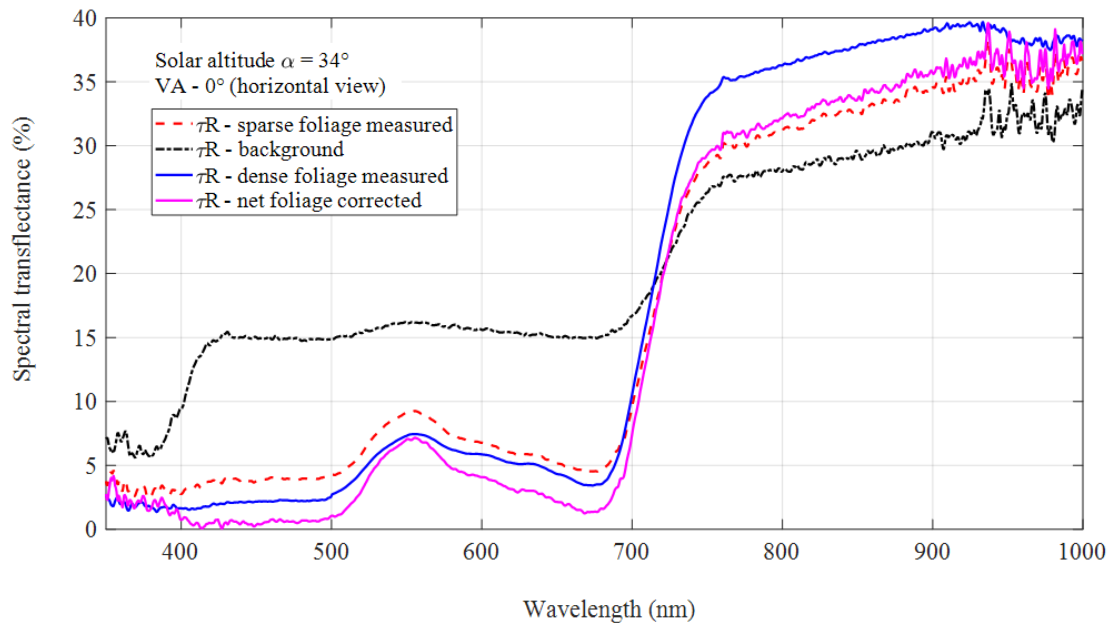
**Original image**

**Adjusted by ImageJ software**  
**Void ratio: VR = 23.3%**

444

445 (b) Void ratio of gaps in the viewing vision determined by the ImageJ software

446



447

448 (c) Net transmittance of foliage excluding gaps compared to measured transmittance

449 **Figure 5.** Tree crown transmittance of a measuring patch with sparse foliage and gaps

450 in a *Tilia platyphyllos* and estimation of the background noise impact with  $\alpha = 34^\circ$ .

451

#### 452 4.2.2 Impact of concave and convex shapes in crown foliage

453 It was found that concave crown contours decreased the  $\tau R$  levels, while the convex

454 contours maximised the  $\tau R$  levels in various tree species. Take the in-situ test of a 5.5

455 m *Sequoiadendron giganteum* tree as an example. Figure 6(a) shows the  $\tau R$

456 measurement of the tree at different heights in the SAz direction ( $\alpha = 37^\circ$ ) with or

457 without concave shapes in the measuring patches. Viewing vision of the fiber-optic tip

458 in tests (red circles in dashed lines represent the vision) was shown in Figure 6(b).

459 Maximum  $\tau R$  appeared at 1.8 m height nearly without concave shapes in the

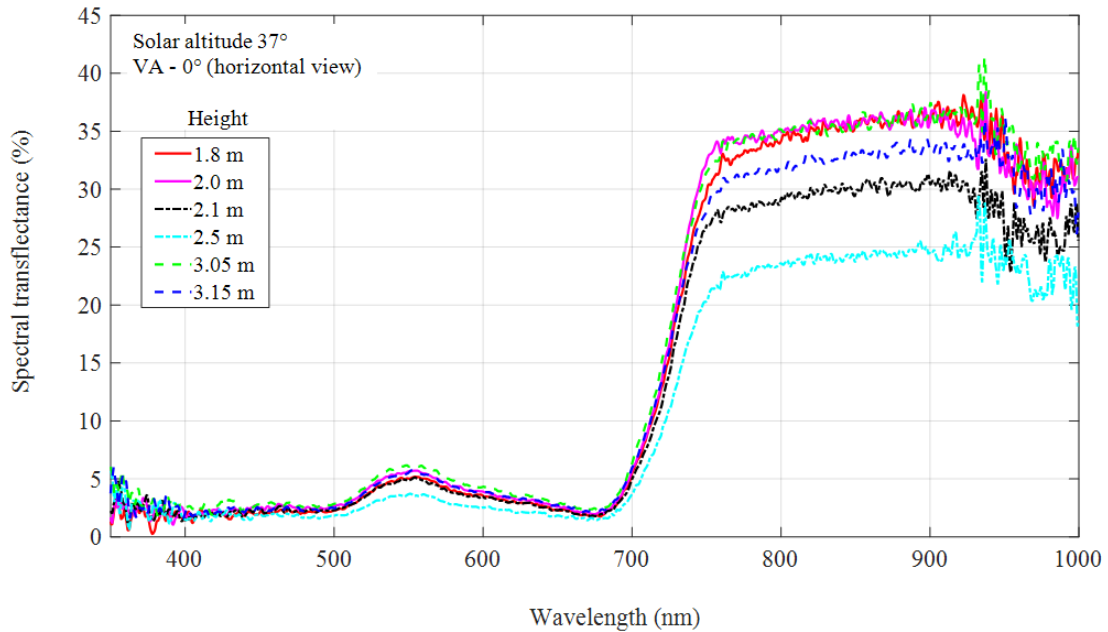
460 measuring patch, while the minimum  $\tau R$  appeared at 2.5 m height with concave

461 shapes accounting for approximately half of the area of the viewing vision, and the  $\tau R$

462 at other heights with concave shapes of different extents fell in between. Foliage gaps

463 were rather small compared to the area of concave shapes in these cases. As sunlight  
464 was captured by concave shapes in the measuring patches, the concave shapes degraded  
465  $\tau R$  levels to different extents depending on the specific scenarios. When the center of  
466 the viewing vision (the circles in Figure 6(b)) deviated from the concave shapes and the  
467 ratio of concave shapes was not big, it only slightly degraded the  $\tau R$  (see  $\tau R$  spectra  
468 at heights of 2.0 m and 2.1 m in Figure 6(a)). It implies that received light of the fiber-  
469 optic tip is not evenly contributed by the viewing vision.

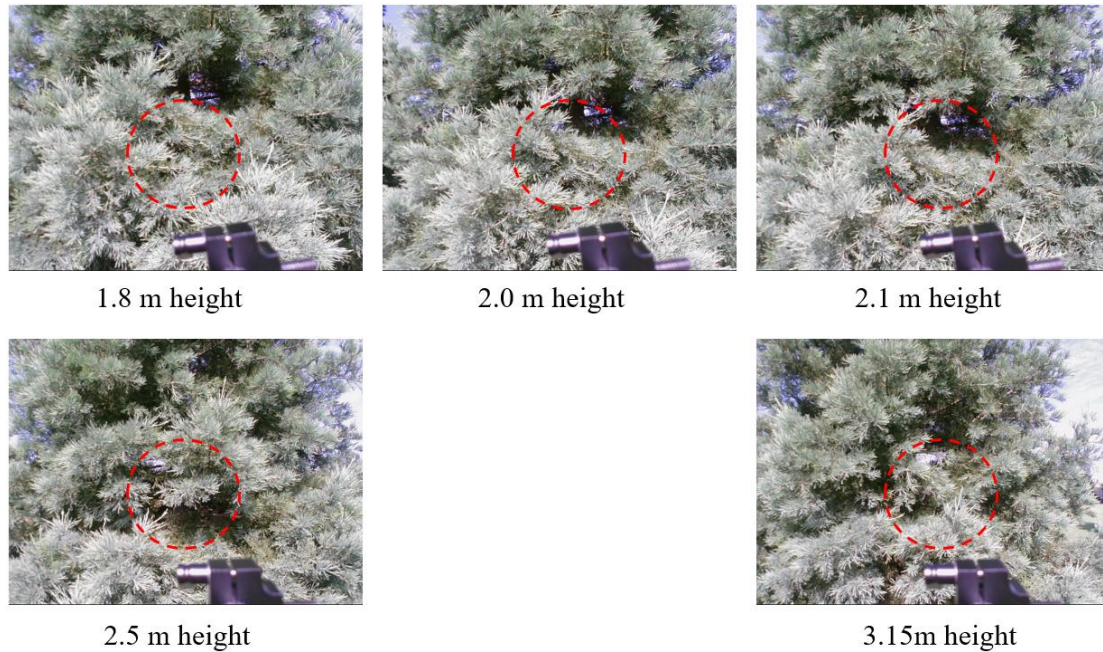
470



471

472

(a)



473

2.5 m height

474

(b)

475 **Figure 6.** Tree crown  $\tau R$  measurement of a *Sequoiadendron giganteum* at different  
 476 heights with or without concave shapes in the measuring patches (a)  $\tau R$  spectra ( $\alpha =$   
 477  $37^\circ$ ); (b) viewing vision of the fiber-optic tip in tests (see red circles in dashed lines).

478

479 The impact of sparse foliage with gaps and concave crown shapes on the transfectance  
 480 is complicated and heterogeneous, and different trees within a species do not share a  
 481 common feature of local foliage distributions. Hence, it is preferable to avoid sampling  
 482 measuring patches that exhibit sparse foliage with gaps and concave contours when  
 483 collecting data for statistical analysis of radiative performance levels of various tree  
 484 species. Any such patches are likely to be identified as outliers in transfectance  
 485 sampling. Generally, it is possible to find measuring patches on trees with relatively  
 486 dense foliage and without visible concave contours. In our field tests of 10 tree species,  
 487 even for the tree species with the sparsest foliage (*Betula pendula* - silver birch) it was

488 easy to find dense foliage for tests without gaps in foliage and concave contours using  
489 the naked-eye.

490

#### 491 **4.2.3 Impact of solar altitude on tree crown $\tau R$**

492 To explore the relationship between change in transfectance and solar time, solar  
493 altitude ( $\alpha$ ) was recorded when sampling the transfectance, referring to a website [72].

494 Figure 7 shows the  $\tau R$  spectra in the frontal sunlit area of a *Carpinus betulus* tree at

495 different solar altitudes. It suggests that the tree crown transfectance increases as solar

496 altitude rises. In further data analysis, it is found that the  $\tau R$  in the IR region tends to

497 be linearly correlated with  $\alpha$ , while no obvious variation is observed in the VIS region

498 due to a low  $\tau R$  level. To dig out laws of change of  $\tau R$  versus  $\alpha$ , mean transfectance

499 in the wavelength range of 800–900 nm ( $\tau R_{mean,800-900}$ ) was taken as an indicator,

500 because tree crown  $\tau R$  spectra usually tend to be flat and hold the maximum spectral

501 transfectance in the NIR wavelength range of 800–900 nm. Figure 8 shows the

502  $\tau R_{mean,800-900}$  of the *Carpinus betulus* trees in terms of the tree crown  $\tau R$  in the

503 frontal sunlit area linearly correlated with solar altitude  $\alpha$ . The rule of change of IR

504 transfectance versus solar altitude allows making a benchmark for intraspecies and

505 interspecies comparisons in section 4.4, by converting  $\tau R$  spectra at different solar

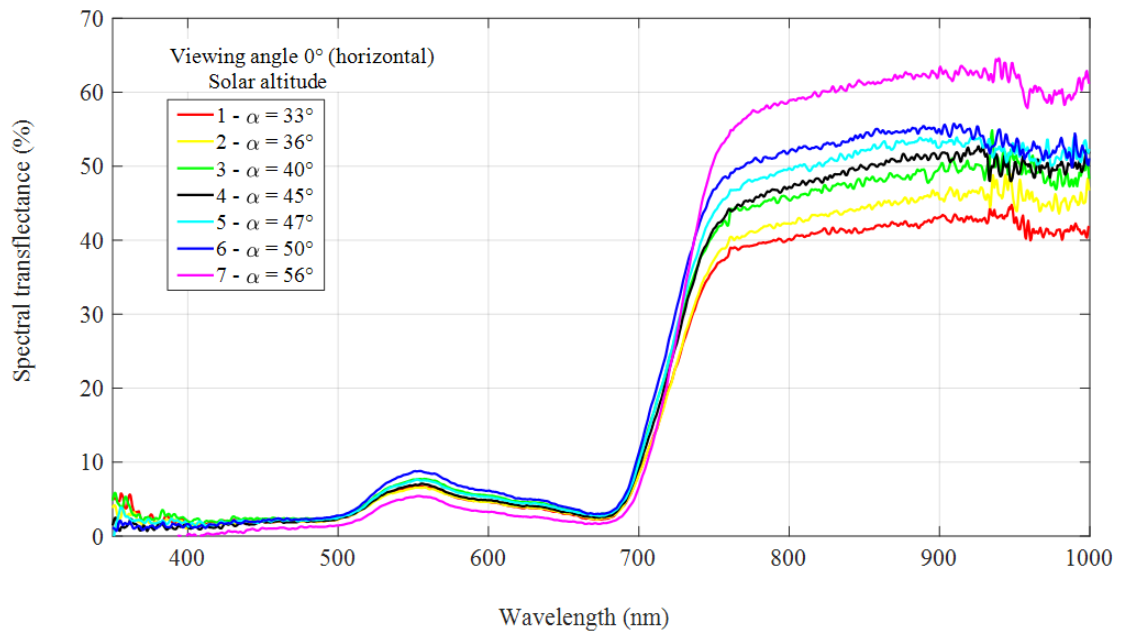
506 altitudes into equivalent  $\tau R$  spectra at the same solar altitude. Figure 9 shows the

507 linear fitting results of the  $\tau R$  spectra in the frontal sunlit area of the *Carpinus betulus*

508 trees varying with solar altitude in the wavelength range of 350–1000 nm.

509

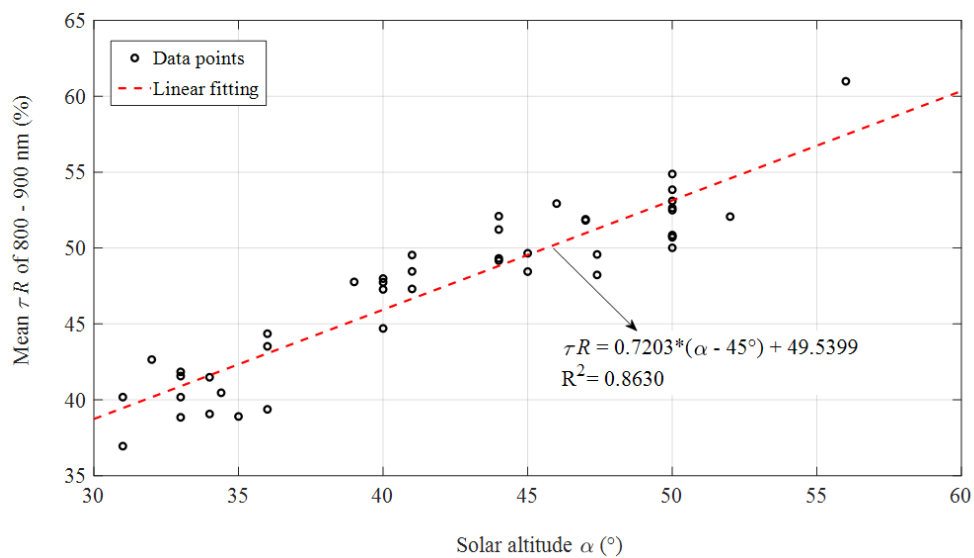
510



511

512 **Figure 7.** Transflectance spectra of tree crown surfaces for a *Carpinus betulus* tree in  
513 the frontal sunlit area at different solar altitudes ( $\alpha$ ).

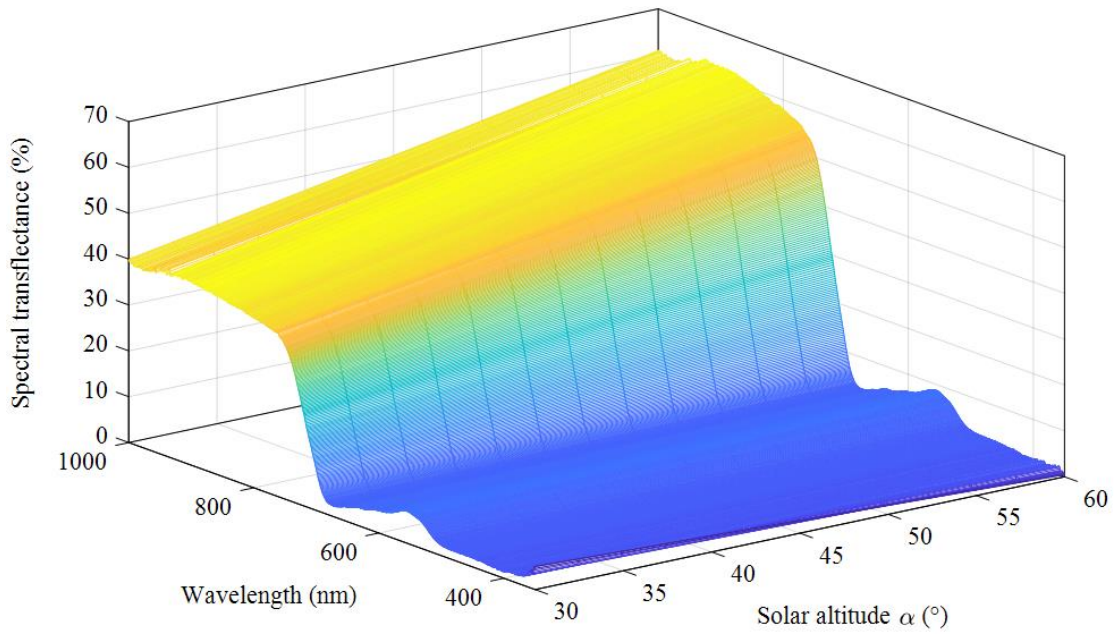
514



515

516 **Figure 8.** Linear fitting of the 800–900 nm mean transmittance ( $\tau R_{mean,800-900}$ ) with  
517 the solar altitude  $\alpha$  for individual *Carpinus betulus* trees using samples in the frontal  
518 sunlit area of trees.

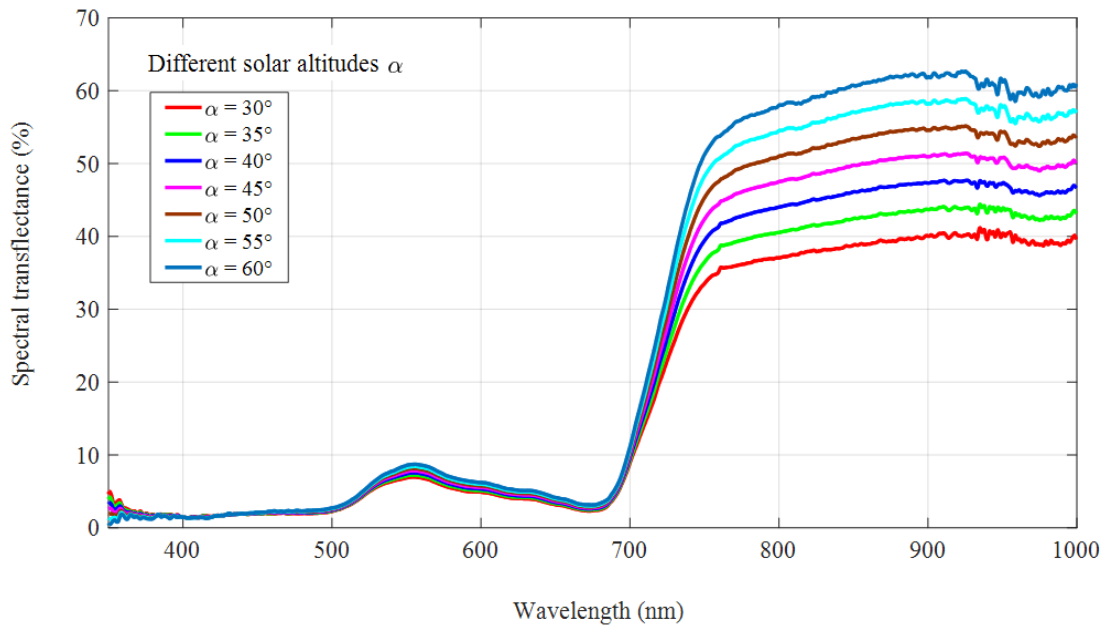
519



520

521

(a) 3D plot



522

523

(b) 2D plot with discrete values of solar altitude

524 **Figure 9.** Linear fitting of tree crown transfectance spectra in the frontal sunlit area of

525 *Carpinus betulus* trees varying with solar altitude in the wavelength range of 350–1000

526 nm.

527



528 In all the ten species measured, it was found that the tree crown IR transfectance in the  
529 frontal sunlit area of trees for a specific species was linearly correlated with solar  
530 altitude on sunny days. The coefficients of determination ( $R^2$ ) in most cases of linear  
531 fittings were above 0.76, except the tree species *Betula pendula* and *Aesculus*  
532 *hippocastanum*. It was presumed that the low  $R^2$  in the fitting of *Betula pendula* was  
533 mainly due to apparently sparse leaf density of the species. As to the species *Aesculus*  
534 *hippocastanum*, the low  $R^2$  in the fitting was attributed to the development of horse  
535 chestnut leaf-miner throughout the summer [73]. Horse chestnut leaf-miner caused  
536 brown blotch mines to develop between the leaf veins, resulting in a degradation of the  
537 transfectance spectrum especially in 750–900 nm wavelength range.

538

### 539 **4.3 Spatial distribution of transfectance around tree crowns**

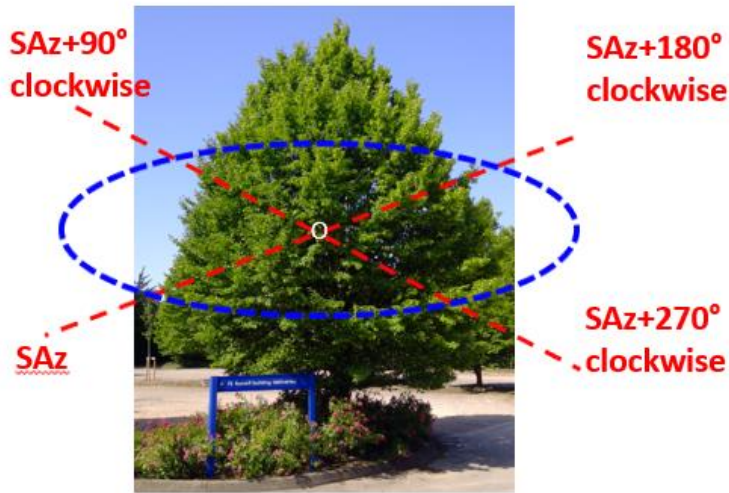
540 As argued in our earlier work [62], transmission and reflection spectra at the leaf level  
541 were similar between trees (similar results also shown in section 4.1), while substantial  
542 variations were found in tree crown  $\tau R$  (transfectance) spectra due to crown structural  
543 difference and solar time. To explore spatial distribution rules of the radiative  
544 performance across a tree crown,  $\tau R$  spectra in typically horizontal and vertical loops  
545 around the tree crowns have been examined.

546

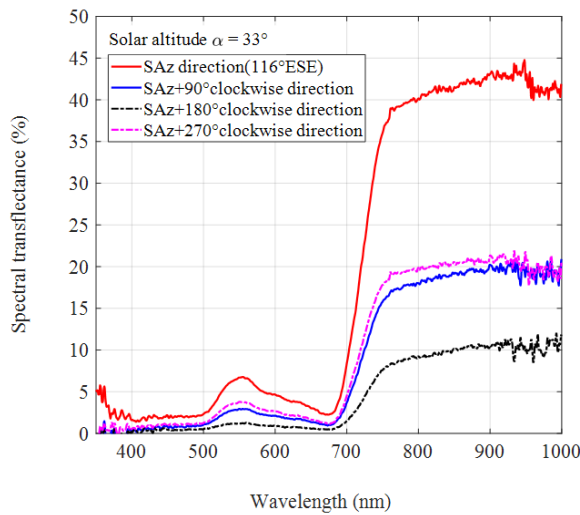
#### 547 **4.3.1 $\tau R$ Distribution in a horizontal loop**

548 Four orientations in a horizontal plane were concerned, as shown in Figure 10(a) with  
549 the 7.0 m height *Carpinus betulus* tree. A single vertical reference plane in the solar

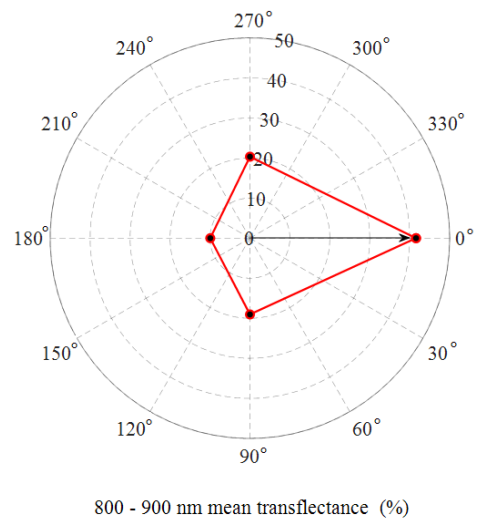
550 azimuth (SAz) direction was chosen for  $\tau R$  spectra measurements in the four  
551 horizontal directions (SAz; SAz +90° clockwise; SAz +180° clockwise; SAz +270°  
552 clockwise). The test sequence was implemented at 4.4 m height during 9:44–9:47 am  
553 (British Summer Time) on the sunny day of 20th August 2019 with solar altitude  $\alpha =$   
554 33°. Figure 10(b) shows measured  $\tau R$  spectra in the four horizontal directions. To  
555 display the transfectance distribution in different directions intuitively, the  
556  $\tau R_{mean,800-900}$  (800–900 nm mean transfectance) was taken as an indicator again.  
557 Figure 10(c) plots the distribution of  $\tau R_{mean,800-900}$  in the horizontal loop in polar  
558 coordinates, where the radius from the origin ‘0’ to the point represents the value of  
559  $\tau R_{mean,800-900}$ . The maximum  $\tau R$  spectrum in the horizontal loop appears in the  
560 frontal sunlit area of the tree, followed by SAz+90° and SAz+270° clockwise directions.  
561 The tree crown  $\tau R$  on the shade side (SAz +180° clockwise) has the lowest  $\tau R$  level.  
562 It seems that the  $\tau R_{mean,800-900}$  in the SAz+90° and SAz+270° directions tends to be  
563 spatially symmetric. This was because no obvious concave contours were viewed on  
564 the measuring patches in both directions. We have observed scenarios of non-  
565 symmetric distribution in the two directions in an *Acer campestre* tree during 10:35–  
566 10:40 am on 27th June 2019, as shown in Figure 11. The  $\tau R_{mean,800-900}$  in the  
567 SAz+270° clockwise direction was much lower than that in the SAz+90° clockwise  
568 direction, as apparent concave contours appeared in the SAz+270° clockwise direction,  
569 resulting in a reduction of the  $\tau R$  level.  
570



(a)



(b)



(c)

571

572

573

574

575 **Figure 10.** Transflectance ( $\tau R$ ) spectra distribution of a *Carpinus betulus* tree in a

576 horizontal loop around the tree crown at  $\alpha = 33^\circ$  (a) sketch of four horizontal

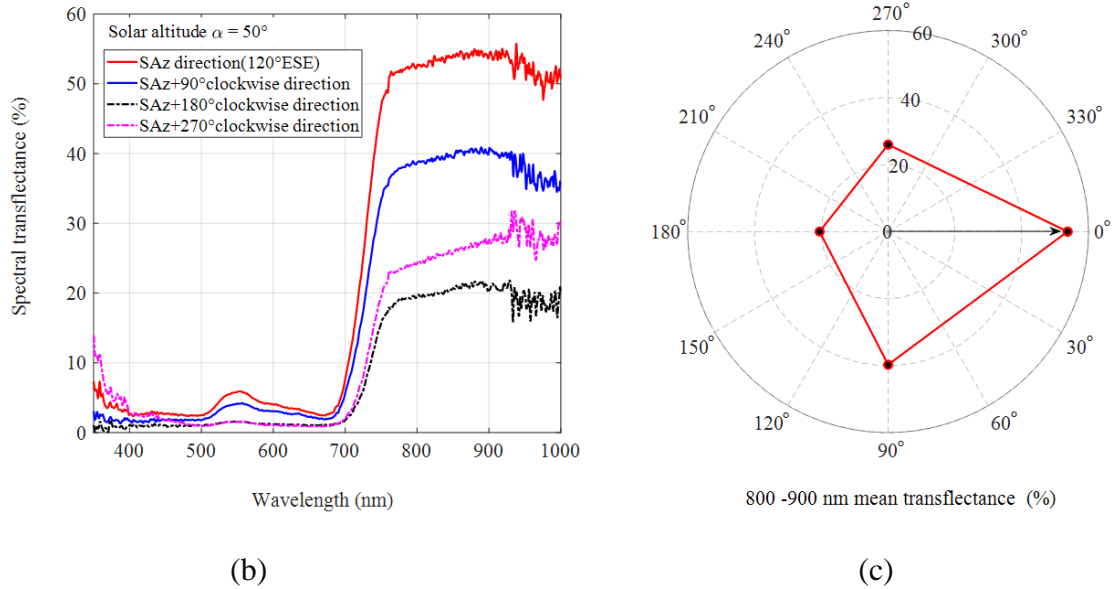
577 directions; (b) measured  $\tau R$  spectra in four directions (SAz – Solar azimuth; ESE –

578 East South East); (c) distribution of  $\tau R_{mean,800-900}$  in polar coordinates ( $0^\circ$  – SAz

579 direction;  $90^\circ$  – SAz +  $90^\circ$  clockwise;  $180^\circ$  – SAz +  $180^\circ$  clockwise;  $270^\circ$  – SAz +  $270^\circ$

580 clockwise).

581



582

(b)

800-900 nm mean transmittance (%)

(c)

584 **Figure 11.** Transflectance ( $\tau R$ ) distribution of an *Acer campestre* tree in a horizontal  
 585 loop around the tree crown at  $\alpha = 50^\circ$  (a) measured  $\tau R$  spectra in four directions; (b)  
 586 distribution of  $\tau R_{mean,800-900}$  in polar coordinates.

587

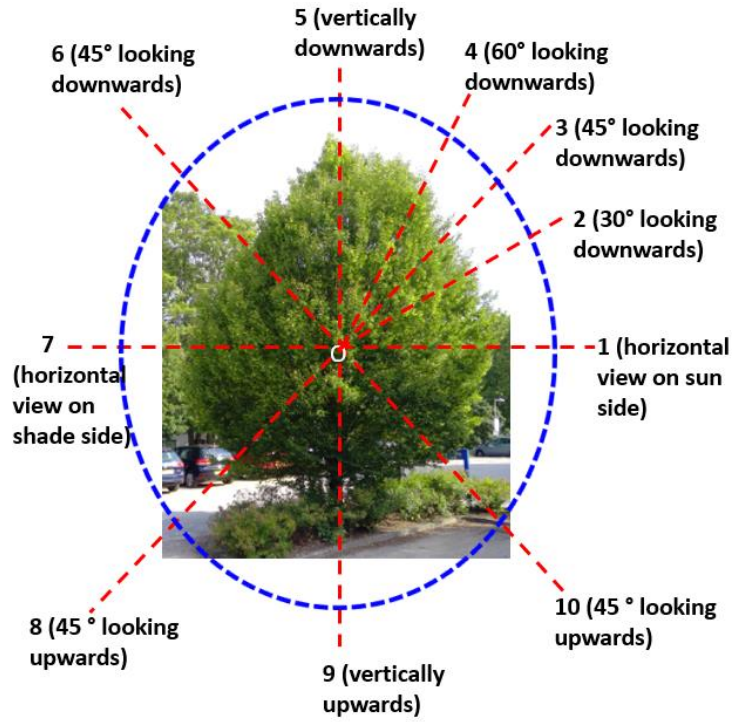
588 **4.3.2  $\tau R$  Distribution in a vertical loop around the tree crown and aligned with**  
 589 **the solar azimuth direction**

590 Two typical vertical loops around the tree crown were chosen in determining  
 591 distribution of tree crown  $\tau R$  (transflectance) in vertical planes. One was a vertical  
 592 loop aligned with the SAz (solar azimuth) direction. The other was a vertical loop  
 593 perpendicular to the SAz direction (see next section 4.3.3). Figure 12(a) sketches 10  
 594 sampled directions distributed in the vertical loop aligned with the SAz in the 7.0 m  
 595 height *Carpinus betulus* tree. Figure 12(b) gives measuring results of the  $\tau R$  spectra  
 596 in the 10 sampled directions with the tree at  $\alpha = 35^\circ$ . The distribution of  
 597  $\tau R_{mean,800-900}$  is delineated in Figure 12(c). It indicates that points ‘1’, ‘2’, ‘3’, ‘4’,  
 598 ‘5’ in the frontal sunlit area of the tree have high  $\tau R$  levels, while other points hold

599 relatively low  $\tau R$  levels. Especially, point '9' beneath the tree has the minimum  
600  $\tau R_{mean,800-900}$  value (only 6.9%). Additionally, the point '4' representing the case of  
601 fiber-optic tip tilted  $60^\circ$  looking downwards has the maximum  $\tau R_{mean,800-900}$ . The  
602 values of  $\tau R_{mean,800-900}$  in the frontal sunlit area at different viewing angles (VA =  
603  $30^\circ$ ,  $45^\circ$ ,  $60^\circ$  and  $90^\circ$  looking downwards) varied with solar time, as it was found that  
604 the maximum value did not maintain in the direction of VA =  $60^\circ$  downwards. Figure  
605 13 gives the vertical loop distribution of the *Carpinus betulus* tree at the solar altitude  
606  $\alpha = 49^\circ$ . Comparing the horizontal samples of point '1' in Figures 12(c) and 13, it  
607 confirmed that the tree crown  $\tau R$  at a higher solar altitude ( $\alpha = 49^\circ$ ) is higher than  
608 that at a lower case ( $\alpha = 35^\circ$ ). Furthermore, the strongest tree crown transfection was  
609 found primarily towards sky on the sunlit side of trees rather than towards zenith.  
610 Infrared transfection towards surrounding buildings and pedestrians is substantial. The  
611 finding provides insights on understanding radiative interactions between urban trees  
612 and surrounding built environments.

613

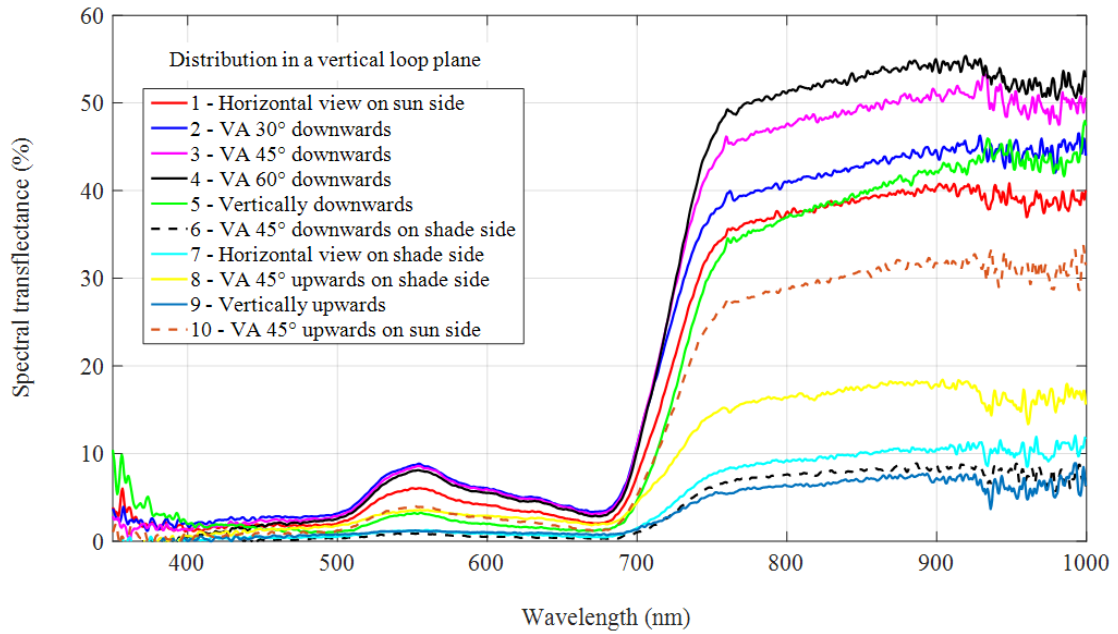
614 Additionally, it is noteworthy that tree crown morphology is linked to the space of the  
615 frontal sunlit area of trees, implying that tree morphology affects distributions of the  
616 tree crown  $\tau R$ .



617

618

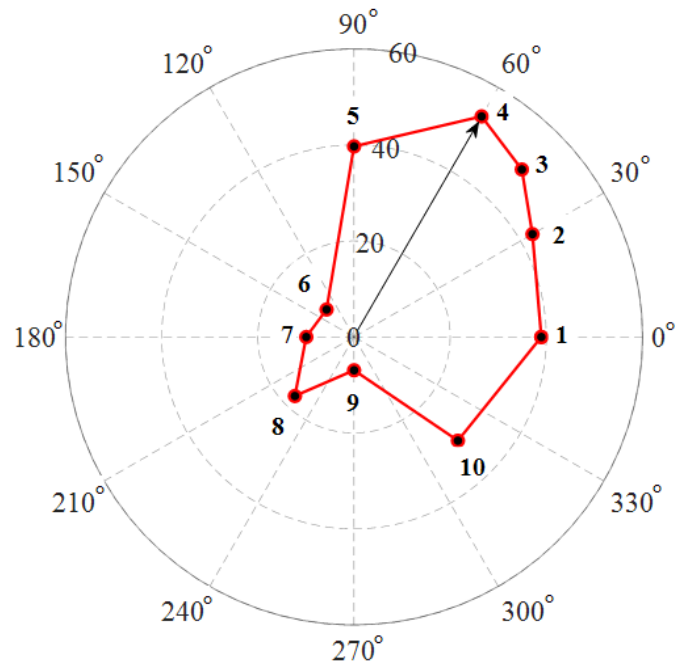
(a)



619

620

(b)



800 - 900 nm mean transmittance (%)

(c)

621

622

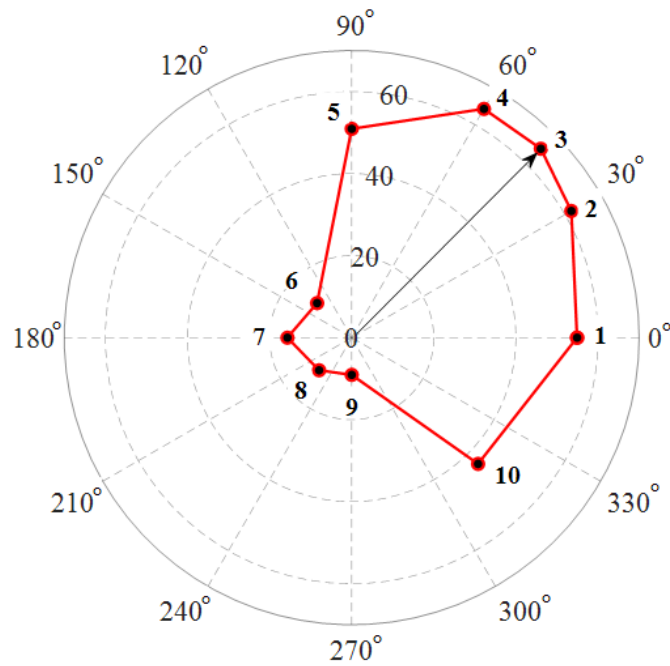
623 **Figure 12.** Transmittance ( $\tau R$ ) spectra distribution of a *Carpinus betulus* tree at  $\alpha =$

624  $35^\circ$  in a vertical loop around tree crown and aligned with the solar azimuth (SAz)

625 direction (a) sketch of 10 sampled directions in the vertical loop; (b) measured  $\tau R$

626 spectra; (c) distribution of  $\tau R_{mean,800-900}$  in polar coordinates.

627



800 - 900 nm mean transfectance (%)

628

629 **Figure 13.**  $\tau R_{mean,800-900}$  distribution of a *Carpinus betulus* tree in polar coordinates

630 at  $\alpha = 49^\circ$  in a vertical loop around the tree crown and aligned with the SAz direction

631

632 **4.3.3  $\tau R$  Distribution in a vertical loop around the tree crown and perpendicular**  
 633 **to the solar azimuth direction**

634 The vertical loop perpendicular to the SAz direction was sampled in 8 directions, as

635 sketched in Figure 14(a). Figure 14(b) gives the measured  $\tau R$  spectra of the *Carpinus*

636 *betulus* tree in the 8 sampled directions at  $\alpha = 37^\circ$ , while Figure 14(b) plots

637 distribution of  $\tau R_{mean,800-900}$  (800–900 nm mean) in polar coordinates. The

638 maximum  $\tau R$  appears at point ‘3’ (vertically downwards), with  $\tau R$  at the other points

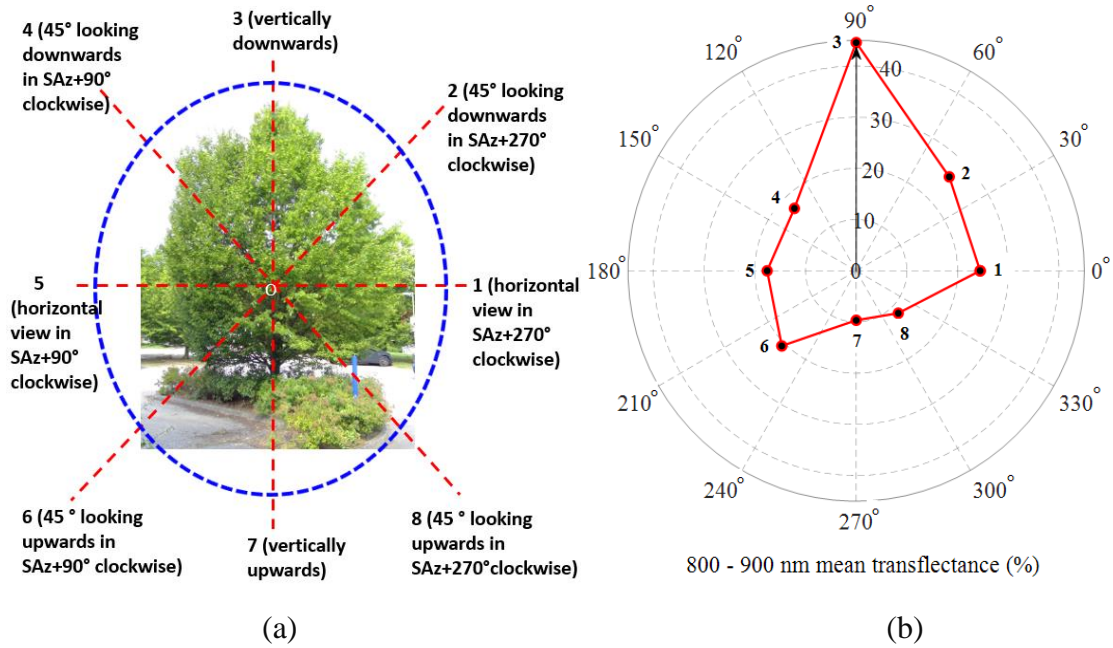
639 (‘1’, ‘2’, ‘4–8’) on lower levels. Comparing Figure 14(b) with the distribution in Figure

640 12(c) neglecting a slight change of solar altitude, it confirms that the primary tree crown

641 transfection is towards sky on the sunlit side of trees rather than towards zenith.

642





643  
644

645 **Figure 14.** Transflectance ( $\tau R$ ) spectra distribution of a *Carpinus betulus* tree at  $\alpha =$   
646  $37^\circ$  in a vertical loop around tree crown and perpendicular to the SAz direction (a)  
647 sketch of 8 sampled directions in the vertical loop;; (b) distribution of  $\tau R_{mean,800-900}$   
648 in polar coordinates.

649

#### 650 4.4 Interspecific difference comparison of radiative performance levels

##### 651 4.4.1 Principles of sample selections in estimating statistical mean $\tau R$ spectra of 652 tree species

653 As elucidated in sections 4.2 and 4.3, the impact factors of the tree crown  $\tau R$  are  
654 diverse, and the spatial distribution of the  $\tau R$  in tree crowns is nonuniform and varies  
655 with solar altitude. A benchmark is therefore needed to make interspecific comparison.  
656 Principles of test sample selections in estimating the statistical mean  $\tau R$  spectra of  
657 various tree species are stated below:

- 658 • Visually dense measuring patches without visible gaps in crown foliage and

659 concave crown contours in the viewing vision of the fiber-optic tip were selected.

660 All trees used in the experiment were young adult to mature adult trees. Tree

661 ages were not accounted for – the only requirement was that dense patches of

662 foliage could be located on the tree crowns.

- 663 • The  $\tau R$  spectra in the frontal sunlit area of trees with vertical reference planes
- 664 normal to transient solar azimuth (SAz) directions were sampled to examine
- 665 intraspecific and interspecific statistical means.
- 666 •  $\tau R$  spectra samples with horizontal views of the fiber-optic tip were selected
- 667 for statistical mean.
- 668 • Solar altitude  $\alpha = 45^\circ$  was chosen as a benchmark condition to compare
- 669 interspecies difference. Measured transfectance spectra at solar altitudes
- 670 different from  $45^\circ$  were converted to equivalent transfectance spectra at  $\alpha =$
- 671  $45^\circ$ , considering linear correlations of transfectance spectra with  $\alpha$  within
- 672 species (referring to section 4.2.3).
- 673 • Usually, at least 3 effective transfectance spectra were sampled for an
- 674 individual tree.
- 675 • At least 5 trees were sampled within a species (except the *Acer platanoides* as
- 676 only four individual trees were considered) to estimate intraspecific statistical
- 677 mean.
- 678 • Through chlorophyll fluorescence and heat stress measurements of part of trees
- 679 selected in the field tests, it showed that the trees were subject to mild or
- 680 moderate physiological stress and no significant effect of the tree physiological

681 stress on the  $\tau R$  was observed. Similarly, no significant effect of different  
682 urbanised settings of tested trees (planted on paved/sealed surfaces or on green  
683 lawns/parks) on the  $\tau R$  was found. Thus, the impact of heat stress and different  
684 urbanized settings of trees was not assessed in intraspecific statistical analysis.

685

#### 686 **4.4.2 Interspecific difference of infrared radiative performance levels**

687 Here we use *Carpinus betulus* as an example to display the process of estimating  
688 statistical mean  $\tau R$  spectrum within a species. In total, effective  $\tau R$  spectrum  
689 samples of 9 *Carpinus betulus* trees were obtained.  $\tau R$  spectra of each individual tree  
690 were converted to the  $\tau R$  spectrum at  $\alpha = 45^\circ$ , and were then averaged to get a  
691 representative  $\tau R$  spectrum for the individual tree. The statistical mean  $\tau R$  spectrum  
692 of the *Carpinus betulus* species was estimated by using 9 representative  $\tau R$  spectra  
693 from 9 individual trees. Representative  $\tau R$  spectra of 5–9 trees were obtained for  
694 various tree species except the *Acer platanoides*, as only four individual trees were  
695 accessible for the copper Norway maple. Statistical mean  $\tau R$  spectra in the frontal  
696 sunlit area of the 10 tree species at  $\alpha = 45^\circ$  can be accessed in **Appendix A**.

697

698 Figure 15 gathers the mean  $\tau R$  spectra and corresponding standard error bands of the  
699 10 species, displaying interspecific performance difference. Table 1 lists statistical  
700  $\tau R_{mean,800-900}$  (800–900 nm mean transfectance) values for the 10 tree species. It  
701 suggests that *Aesculus hippocastanum* and *Platanus x acerifolia* have the highest levels  
702 of IR radiative performance ( $\tau R_{mean,800-900}$ :  $0.597 \pm 0.027$  for *Aesculus hippocastanum*

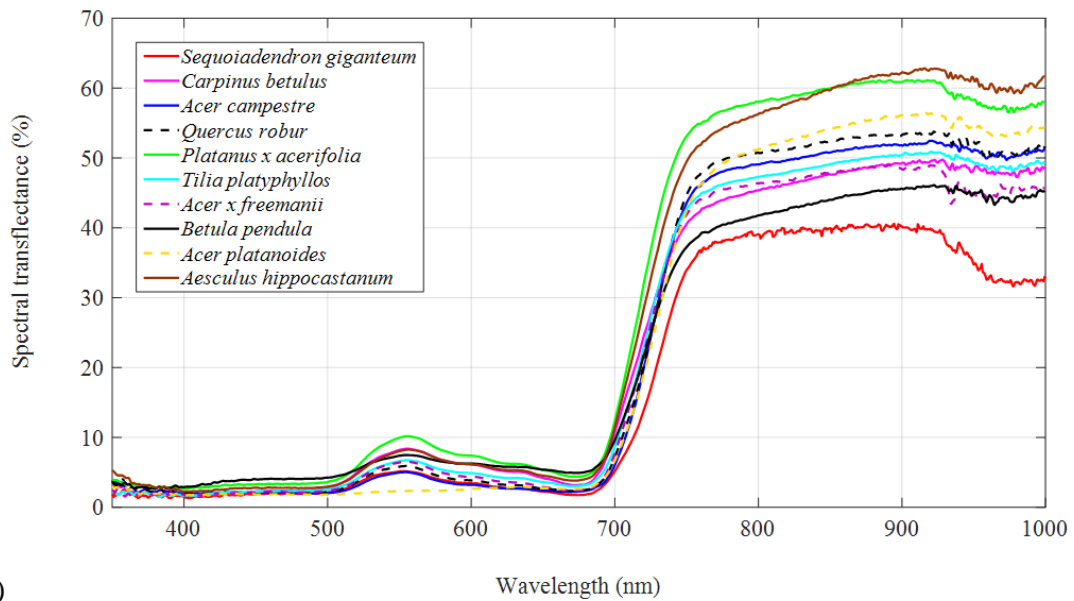
703 and  $0.598 \pm 0.011$  for *Platanus x acerifolia*), followed by *Acer platanoides*, *Quercus*  
704 *robur*, *Acer campestre*, *Tilia platyphyllos*, *Carpinus betulus* (fastigate hornbeam) and  
705 *Acer x freemanii* successively on moderate levels ( $\tau R_{mean,800-900}$ : 0.475–0.540 and  
706 standard error within  $\pm 0.014$ ). *Betula pendula* has the second lowest levels of IR  
707 radiative performance ( $\tau R_{mean,800-900}$ :  $0.439 \pm 0.009$ ), presumably due to the fact that  
708 this native British tree species is usually observed with a small leaf size and apparently  
709 sparse leaf density. *Sequoiadendron giganteum* has the minimum levels of IR radiative  
710 performance ( $\tau R_{mean,800-900}$ :  $0.398 \pm 0.009$ ), resulting from the minimum leaf size  
711 (needle leaves) among the tested species.

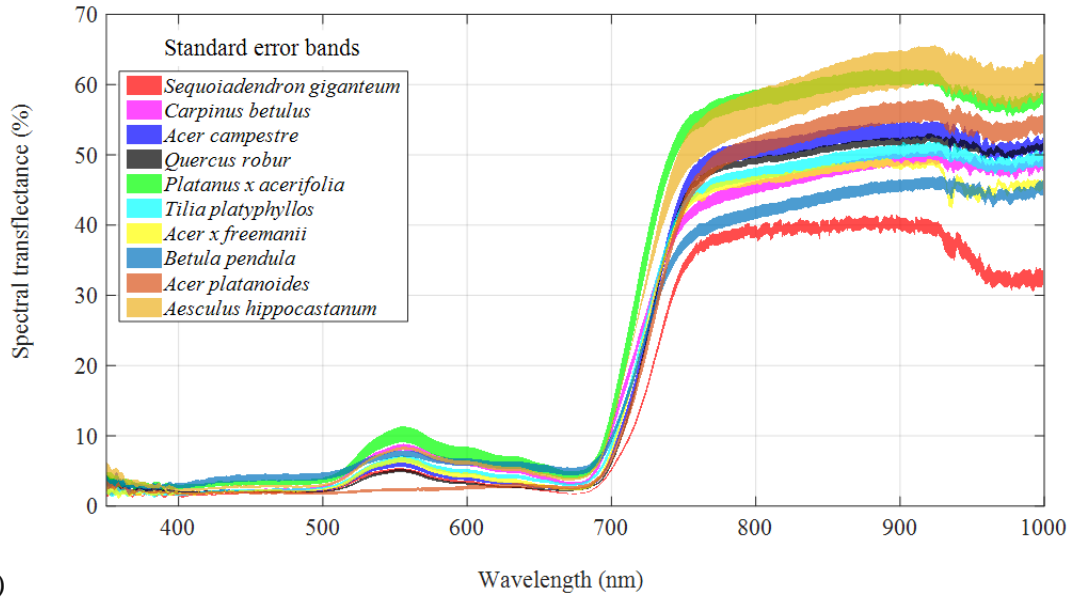
712

713 Figure 16 shows images of tree leaves for the tested species corresponding to the  
714 radiative performance levels. Interesting is that, the tree species with large-sized leaves  
715 (such as *Platanus x acerifolia*, *Aesculus hippocastanum*) lead to maximum radiative  
716 performance levels, followed by the tree species with moderate-sized leaves (e.g. *Acer*  
717 *platanoides*, *Quercus robur*, *Acer campestre*, *Tilia platyphyllos*). *Carpinus betulus* has  
718 a leaf size smaller than other tree species on the moderate levels of radiative  
719 performance, resulting in a slightly lower performance level than the others except *Acer*  
720 *x freemanii*. Although the leaf size of *Acer x freemanii* seems to be close to that of  
721 *Quercus robur* and *Acer campestre*, branching structure of its leaves degrades its  
722 radiative performance level. From this perspective, each individual leaf of *Acer x*  
723 *freemanii* can be viewed as three leaflets which have similar leaf sizes as the *Carpinus*  
724 *betulus* leaves, resulting in the same radiative performance level as the latter.

725 *Sequoiadendron giganteum* with the smallest needle leaves among the 10 species has  
 726 the minimum radiative performance level. It reveals that interspecific difference of  
 727 infrared radiative performance levels strongly depends on leaf size when visibly dense  
 728 foliage (no visible gaps and concave shapes in crown foliage) is observed on the tree  
 729 crown contours. The finding confirms the viewpoint in [74] that species average leaf  
 730 size is the most important determinant of self-shading that affected light capture. It  
 731 provides insights on species selection for heat stress mitigation in urban microclimates.  
 732 The impact of leaf size implies that disregarding tree ages (young or old) in sampling  
 733 visually dense measuring patches (see 4.4.1) is appropriate, as mature trees of a  
 734 specific-species tend to have reasonably similar leaf shape and leaf size.

735





737 (b)

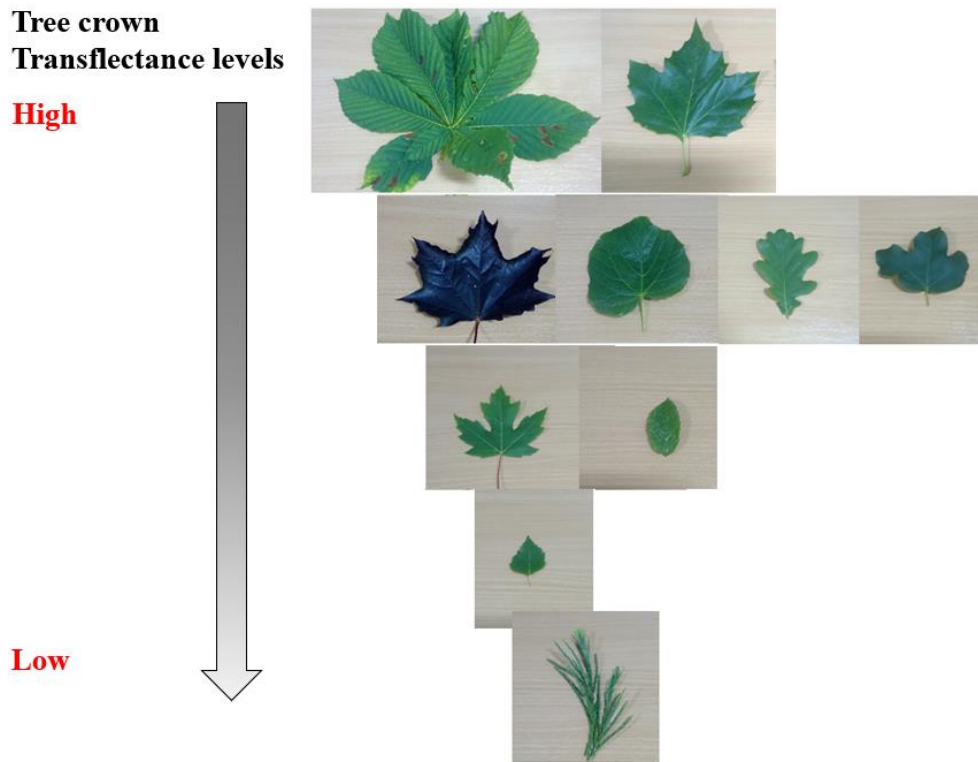
738 **Figure 15.** Interspecific radiative performance difference of ten tree species planted in  
 739 the UK in terms of equivalent  $\tau R$  spectra at  $\alpha = 45^\circ$  (a) statistical mean  $\tau R$  spectra;  
 740 (b) standard mean error bands.

741

742 **Table 1.** Statistical  $\tau R_{mean,800-900}$  for ten tree species

Tree species	$\tau R_{mean,800-900}$ (%)	Standard mean error (%)
<i>Sequoiadendron giganteum</i> (Giant sequoia)	39.8	$\pm 0.9$
<i>Carpinus betulus</i> (Fastigiata hornbeam)	47.5	$\pm 0.9$
<i>Acer campestre</i> (Field maple)	52.2	$\pm 1.2$
<i>Quercus robur</i> (English oak)	50.7	$\pm 0.5$
<i>Platanus x acerifolia</i> (London plane)	59.8	$\pm 1.1$
<i>Tilia platyphyllos</i> (Large-leaved lime)	49.0	$\pm 0.9$
<i>Acer x freemanii</i> (Autumn blaze maple)	47.8	$\pm 0.6$
<i>Betula pendula</i> (Silver Birch)	43.9	$\pm 0.9$
<i>Acer platanoides</i> (Copper Norway maple)	54.0	$\pm 1.4$
<i>Aesculus hippocastanum</i> (Horse chestnut)	59.7	$\pm 2.7$

743



744

745 **Figure 16.** Radiative performance levels of multiple tree species classified by leaf size.

746

747 **4.4.3 Identification of intraspecific and interspecific differences in canopy**  
 748 **transflectance by PCA**

749 At the scale of crown patches significant differences in transflectance were observed

750 between species, and these corresponded to different biological and spectral properties.

751 PCA of the 5 nm spectral bands ( $n = 130$  per tree crown) collected from 67 individual

752 trees across 10 species revealed significant interspecific differences in crown

753 transflectance for the 350-1000 nm range. The first two PCA axes explained 86.9% of

754 the variance in spectral profiles and were significantly correlated with different canopy

755 transflectance properties (see Table 2).

756

757 **Table 2.** Relationship between first five PCA axes and bands of canopy transflectance

758 in the 350-1000 nm range across 67 individual trees drawn from 10 species

Axis	Variance explained	Cumulative variance	Positive correlation (r)	Negative correlation (r)
1	54.5%	54.5%	All except 370-375 nm	
2	32.4%	86.9%	735-1000 nm	395-705 nm
3	7.2%	94.1%	350-485 nm	525-615 & 695-735 nm
4	2.6%	96.7%	350-400 nm	
5	1.5%	98.2%	350-355 nm	

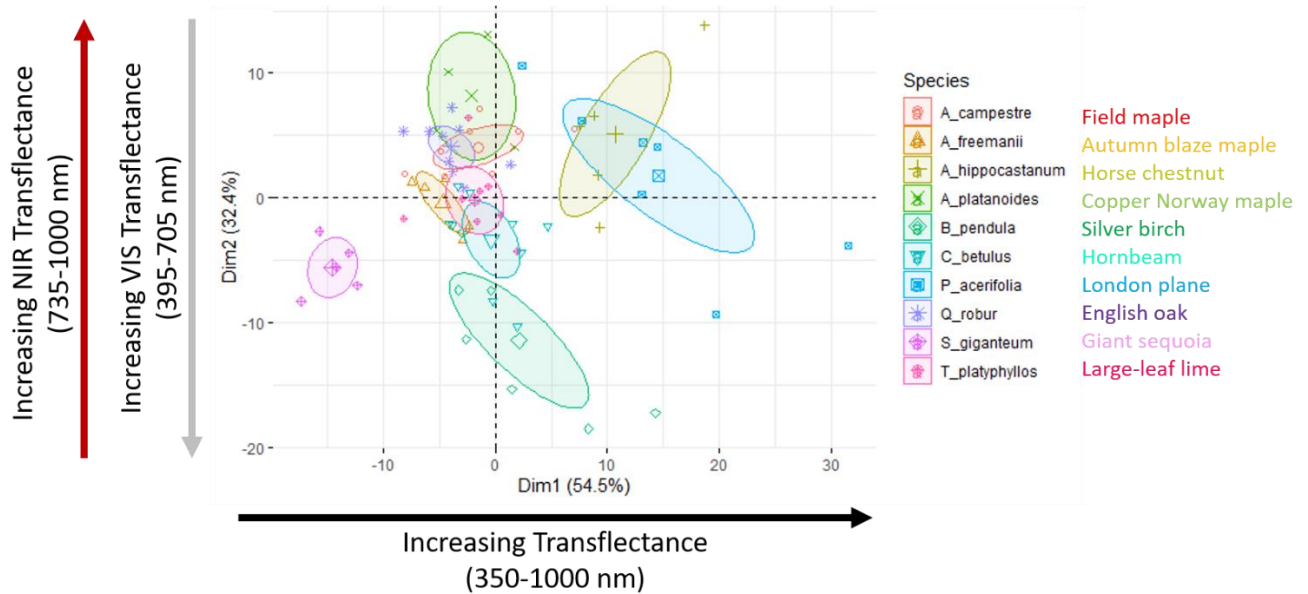
759

760 Increasing transreflectance in the 350-1000 nm range corresponded to axis 1 of the PCA  
761 and was the most explanatory factor contributing to species differences (Table 2). The  
762 strongest correlation to axis 1 was found in the transition between VIS and NIR; large-  
763 leaved species (*Platanus x acerifolia* and *Aesculus hippocastanum*) were positively  
764 associated with this axis, whereas the only conifer (*Sequoiadendron giganteum*) was  
765 negatively associated (Species  $R^2 = 0.731$ ;  $P < 0.001$ ; Figure 17). Species were further  
766 sub-divided by their opposing interactions with NIR and components of VIS. Axis 2  
767 corresponded with increasing NIR and decreasing VIS (violet, blue, yellow and orange)  
768 transreflectance (Table 2); *Acer platanoides* and *Quercus robur* were positively  
769 associated with this second axis, whereas *Sequoiadendron giganteum* and *Betula*  
770 *pendula* were negatively associated (Species  $R^2 = 0.663$ ;  $P < 0.001$ ; Figure 17). These  
771 results show that interspecific differences between the transreflectance profiles of  
772 commonly planted tree species are readily measurable and reveal key differences  
773 between species that can alter radiative performance in urban areas. As noted by  
774 Cavender-Barres *et al.* [70], leaf spectra can be considered as an integrated measure of  
775 phenotype; hence, further research into the impacts of environmental stress on canopy  
776 transreflectance could help in understanding the likely consequences of climate change



777 for urban areas, in terms of the impact on radiative performance and energy balance.

778



779

780 **Figure 17.** PCA of crown transreflectance spectra for axes 1 and 2 displaying  
781 differentiation between species and spectral properties correlated with each axis.

782 Polygons represent 95% confidence interval for each species.

783

784 Furthermore, PERMANOVA using distance indices supported significant interspecific

785 variation in crown transreflectance (Species, 999 permutations:  $Pseudo-F_{df\ 9,57} = 14.3$ ;

786  $R^2 = 0.694$ ;  $P = 0.001$ ). Although variability in crown transreflectance was observed

787 within species, examination of the homogeneity of multivariate dispersion indicated

788 that intraspecific variance (i.e. variance within species) was not significantly different

789 between species (Species, 999 permutations:  $F_{df9,57} = 1.86$ ;  $P = 0.077$ ). Hence, crown

790 transreflectance values were relatively similar within species, and the degree of

791 multivariate variability within species was relatively similar between species. However,

792 this observation was based on collecting spectral data from canopy patches with a

793 consistent, generally convex, coverage of leaves and avoiding gaps or concave patches.  
794 Therefore, intraspecific differences are expected to be strongly influenced by their  
795 unique life-history, including interactions with the biotic/abiotic environment and local  
796 government landscaping and management decisions.

797

## 798 **5 Conclusions**

799 Based on a tree crown spectroscopy measurement method established earlier,  
800 substantial in-situ tests of radiative performance of 10 tree species have been  
801 implemented in terms of the tree crown transfectance ( $\tau R$ ). Spatial distribution rules  
802 of the  $\tau R$  across tree crowns were identified. Infrared radiative performance difference  
803 of the 10 tree species (*Sequoiadendron giganteum*, *Carpinus betulus*, *Acer campestre*,  
804 *Quercus robur*, *Platanus x acerifolia*, *Tilia platyphyllos*, *Acer x freemanii*, *Betula*  
805 *pendula*, *Acer platanoides*, *Aesculus hippocastanum*) commonly planted in the UK was  
806 statistically determined in terms of  $\tau R$  spectra in frontal sunlit area of the trees, by  
807 converting  $\tau R$  spectra on the same benchmark of solar altitude  $\alpha = 45^\circ$ . Main  
808 findings are as follows:

- 809 • Mean leaf reflectance spectra of various tree species have a minor difference  
810 between each other, with spectral reflectance deviations of  $\pm 4\%$ , contrasting to  
811 substantial differences in spatial distribution of the  $\tau R$  across the tree crowns.
- 812 • Impact factors of tree crown transfectance (sparse foliage with gaps in crown  
813 foliage, concave and convex shapes in crown foliage, solar time): Visibly non-  
814 uniform foliage distribution in the measuring patches, such as sparse foliage

815 with gaps and concave shapes degrades  $\tau R$  levels to different extents. Impact  
816 of sparse foliage with gaps and concave shapes on  $\tau R$  is complicated and  
817 heterogeneous.  $\tau R$  in the frontal sunlit area of trees for a specific species is  
818 linearly correlated with solar altitude on sunny days, allowing this to be used as  
819 a benchmark for comparing differences in intraspecific and interspecific  
820 performance.

821 • Spatial distribution rules: The primary tree crown  $\tau R$  in a horizontal loop  
822 around tree crowns appears in the frontal sunlit area (SAz direction), followed  
823 by those in SAz+90° and SAz +270° clockwise directions. The  $\tau R$  on the tree  
824 shade side (SAz+180° clockwise) has the lowest levels).  $\tau R$  distributions in  
825 two typically vertical loops perpendicular to each other confirm that the  
826 strongest tree crown transflexion was found primarily towards sky on the sunlit  
827 side of trees rather than towards zenith. The direction of the maximum  
828 transflexion in the frontal sunlit area varies with solar time and depends on the  
829 polar angle consisting of solar azimuth and solar altitude. The  $\tau R$  beneath trees  
830 has the minimum level.

831 • Interspecific difference comparison of infrared radiative performance levels  
832 indicates that tree species such as *Platanus x acerifolia* and *Aesculus*  
833 *hippocastanum* with large-sized leaves, lead to maximum radiative performance  
834 levels, followed by the tree species with moderate-sized leaves (e.g. *Acer*  
835 *platanooides*, *Acer campestre*, *Quercus robur*, *Tilia platyphyllos*).  
836 *Sequoiadendron giganteum* has the minimum radiative performance level,

837 mainly due to its small needle leaves. It reveals that interspecific difference of  
838 the infrared radiative performance levels strongly depends on leaf size if  
839 visually dense foliage (no obvious gaps in foliage and no concave shapes) is  
840 observed on the tree crown contours.

841

842 The findings provide insights on understanding radiative interactions between urban  
843 trees and the surrounding built environments.

844

#### 845 **Acknowledgment**

846 This work is funded by the UK EPSRC/NERC project titled 'InfruTreeCity:  
847 Understanding Infrared radiative performance of urban trees for better future city'  
848 (Grant number: EP/P023819/1). The authors wish to thank Dr. Christos H. Halios at the  
849 University of Reading for demonstrating usages of the Arborcheck instruments in  
850 measuring chlorophyll fluorescence and tree physiological stress, the Evolution  
851 Spectrometers (model SM2500) as well as some other technical assistance. It is also  
852 grateful for the advisory panel members who have attended our meetings to provide  
853 valuable advices. Gratitude is also given to Mr. Rupert Taylor at the University of  
854 Reading, who helped to identify names of tree species in tests.

855

856 **Appendix A. Supplementary materials**

857 Supplementary data associated with this article is openly available in the University of  
858 Reading Research Data Archive, in the online version, at:  
859 <http://dx.doi.org/10.17864/1947.231>. Metadata will be available by request.

860

861 **Declaration of interest: none.**

862

863 **References**

- 864 [1] R. Garcia-Herrera, J. Díaz, R.M. Trigo, J. Luterbacher, E.M. Fischer, A review  
865 of the european summer heat wave of 2003, *Crit. Rev. Environ. Sci. Technol.* 40  
866 (2010) 267–306. <https://doi.org/10.1080/10643380802238137>.
- 867 [2] IPCC, *Climate Change 2014: Synthesis Report. Contribution of Working Groups*  
868 *I, II and III to the Fifth Assessment Report of the Intergovernmental Panel on*  
869 *Climate Change*, 2014.
- 870 [3] A. Gasparrini, B. Armstrong, The impact of heat waves on mortality,  
871 *Epidemiology.* (2011). <https://doi.org/10.1097/EDE.0b013e3181fdcd99>.
- 872 [4] Y. Guo, A. Gasparrini, B.G. Armstrong, *et al.*, Heat wave and mortality: A  
873 multicountry, multicomunity study, *Environ. Health Perspect.* (2017).  
874 <https://doi.org/10.1289/EHP1026>.
- 875 [5] E.M. Fischer, R. Knutti, Anthropogenic contribution to global occurrence of  
876 heavy-precipitation and high-temperature extremes, *Nat. Clim. Chang.* 5 (2015)  
877 560–564. <https://doi.org/10.1038/nclimate2617>.
- 878 [6] L. Zhao, M. Oppenheimer, Q. Zhu, J.W. Baldwin, K.L. Ebi, E. Bou-Zeid, K.

- 879 Guan, X. Liu, Interactions between urban heat islands and heat waves, *Environ.*  
880 *Res. Lett.* 13 (2018) 034003. <https://doi.org/10.1088/1748-9326/aa9f73>.
- 881 [7] C.C. Konijnendijk, K. Nilsson, T.B. Randrup, J. Schipperijn, *Urban forests and*  
882 *trees: A reference book*, 2005. <https://doi.org/10.1007/3-540-27684-X>.
- 883 [8] R. Upreti, Z.H. Wang, J. Yang, Radiative shading effect of urban trees on cooling  
884 the regional built environment, *Urban For. Urban Green.* 26 (2017) 18–24.  
885 <https://doi.org/10.1016/j.ufug.2017.05.008>.
- 886 [9] Z. Zou, Y. Yang, G.Y. Qiu, Quantifying the evapotranspiration rate and its  
887 cooling effects of urban hedges based on three-temperature model and infrared  
888 remote sensing, *Remote Sens.* 11 (2019) 1–18.  
889 <https://doi.org/10.3390/rs11020202>.
- 890 [10] M. Taleghani, Outdoor thermal comfort by different heat mitigation strategies-  
891 A review, *Renew. Sustain. Energy Rev.* 81 (2018) 2011–2018.  
892 <https://doi.org/10.1016/j.rser.2017.06.010>.
- 893 [11] L. Kong, K.K.L. Lau, C. Yuan, Y. Chen, Y. Xu, C. Ren, E. Ng, Regulation of  
894 outdoor thermal comfort by trees in Hong Kong, *Sustain. Cities Soc.* 31 (2017)  
895 12–25. <https://doi.org/10.1016/j.scs.2017.01.018>.
- 896 [12] Z.H. Wang, X. Zhao, J. Yang, J. Song, Cooling and energy saving potentials of  
897 shade trees and urban lawns in a desert city, *Appl. Energy.* 16 (2016) 437–444.  
898 <https://doi.org/10.1016/j.apenergy.2015.10.047>.
- 899 [13] S. Gillner, J. Vogt, A. Tharang, S. Dettmann, A. Roloff, Role of street trees in  
900 mitigating effects of heat and drought at highly sealed urban sites, *Landsc. Urban*

- 901 Plan. 143 (2015) 33–42. <https://doi.org/10.1016/j.landurbplan.2015.06.005>.
- 902 [14] H. Lee, H. Mayer, L. Chen, Contribution of trees and grasslands to the mitigation  
903 of human heat stress in a residential district of Freiburg, Southwest Germany,  
904 *Landsc. Urban Plan.* 148 (2016) 37–50.  
905 <https://doi.org/10.1016/j.landurbplan.2015.12.004>.
- 906 [15] A.S. Yang, Y.H. Juan, C.Y. Wen, C.J. Chang, Numerical simulation of cooling  
907 effect of vegetation enhancement in a subtropical urban park, *Appl. Energy*. 192  
908 (2017) 178–200. <https://doi.org/10.1016/j.apenergy.2017.01.079>.
- 909 [16] D.E. Bowler, L. Buyung-Ali, T.M. Knight, A.S. Pullin, Urban greening to cool  
910 towns and cities: A systematic review of the empirical evidence, *Landsc. Urban*  
911 *Plan.* 97 (2010) 147–155. <https://doi.org/10.1016/j.landurbplan.2010.05.006>.
- 912 [17] W. Zhou, J. Wang, M.L. Cadenasso, Effects of the spatial configuration of trees  
913 on urban heat mitigation: A comparative study, *Remote Sens. Environ.* 195 (2017)  
914 1–12. <https://doi.org/10.1016/j.rse.2017.03.043>.
- 915 [18] S. Sodoudi, H. Zhang, X. Chi, F. Müller, H. Li, The influence of spatial  
916 configuration of green areas on microclimate and thermal comfort, *Urban For.*  
917 *Urban Green.* 34 (2018) 85–96. <https://doi.org/10.1016/j.ufug.2018.06.002>.
- 918 [19] Z. Tan, K.K.L. Lau, E. Ng, Urban tree design approaches for mitigating daytime  
919 urban heat island effects in a high-density urban environment, *Energy Build.* 114  
920 (2016) 265–274. <https://doi.org/10.1016/j.enbuild.2015.06.031>.
- 921 [20] T. Zölch, M.A. Rahman, E. Pfliegerer, G. Wagner, S. Pauleit, Designing public  
922 squares with green infrastructure to optimize human thermal comfort, *Build.*

- 923 Environ. 149 (2019) 640–654. <https://doi.org/10.1016/j.buildenv.2018.12.051>.
- 924 [21] E. Jamei, P. Rajagopalan, M. Seyedmahmoudian, Y. Jamei, Review on the impact  
925 of urban geometry and pedestrian level greening on outdoor thermal comfort,  
926 Renew. Sustain. Energy Rev. 54 (2016) 1002–1017.  
927 <https://doi.org/10.1016/j.rser.2015.10.104>.
- 928 [22] Y. Wang, U. Berardi, H. Akbari, Comparing the effects of urban heat island  
929 mitigation strategies for Toronto, Canada, Energy Build. 114 (2016) 2–19.  
930 <https://doi.org/10.1016/j.enbuild.2015.06.046>.
- 931 [23] Y. Liu, D.J. Harris, Effects of shelterbelt trees on reducing heating-energy  
932 consumption of office buildings in Scotland, Appl. Energy. 85 (2008) 115–127.  
933 <https://doi.org/10.1016/j.apenergy.2007.06.008>.
- 934 [24] J.L. Moss, K.J. Doick, S. Smith, M. Shahrestani, Influence of evaporative  
935 cooling by urban forests on cooling demand in cities, Urban For. Urban Green.  
936 37 (2019) 65–73. <https://doi.org/10.1016/j.ufug.2018.07.023>.
- 937 [25] C.M. Hsieh, J.J. Li, L. Zhang, B. Schwegler, Effects of tree shading and  
938 transpiration on building cooling energy use, Energy Build. 159 (2018) 382–397.  
939 <https://doi.org/10.1016/j.enbuild.2017.10.045>.
- 940 [26] N. Bréda, V. Badeau, Forest tree responses to extreme drought and some biotic  
941 events: Towards a selection according to hazard tolerance?, Comptes Rendus -  
942 Geosci. 340 (2008) 651–662. <https://doi.org/10.1016/j.crte.2008.08.003>.
- 943 [27] C. Calfapietra, J. Peñuelas, Ü. Niinemets, Urban plant physiology: Adaptation-  
944 mitigation strategies under permanent stress, Trends Plant Sci. 20 (2015) 72–75.



- 945 <https://doi.org/10.1016/j.tplants.2014.11.001>.
- 946 [28] R. Teskey, T. Wertin, I. Bauweraerts, M. Ameye, M.A. McGuire, K. Steppe,  
947 Responses of tree species to heat waves and extreme heat events, *Plant Cell*  
948 *Environ.* 38 (2015) 1699–1712. <https://doi.org/10.1111/pce.12417>.
- 949 [29] I. Bauweraerts, M. Ameye, T.M. Wertin, M.A. McGuire, R.O. Teskey, K. Steppe,  
950 Water availability is the decisive factor for the growth of two tree species in the  
951 occurrence of consecutive heat waves, *Agric. For. Meteorol.* 189–190 (2014) 19–  
952 29. <https://doi.org/10.1016/j.agrformet.2014.01.001>.
- 953 [30] S. Leuzinger, R. Vogt, C. Körner, Tree surface temperature in an urban  
954 environment, *Agric. For. Meteorol.* 150 (2010) 56–62.  
955 <https://doi.org/10.1016/j.agrformet.2009.08.006>.
- 956 [31] S. Zheng, J.M. Guldmann, Z. Liu, L. Zhao, Influence of trees on the outdoor  
957 thermal environment in subtropical areas: An experimental study in Guangzhou,  
958 China, *Sustain. Cities Soc.* 42 (2018) 482–497.  
959 <https://doi.org/10.1016/j.scs.2018.07.025>.
- 960 [32] M.A. Irmak, S. Yilmaz, E. Mutlu, H. Yilmaz, Assessment of the effects of  
961 different tree species on urban microclimate, *Environ. Sci. Pollut. Res.* 25 (2018)  
962 15802–15822. <https://doi.org/10.1007/s11356-018-1697-8>.
- 963 [33] C.Y. Park, D.K. Lee, E.S. Krayenhoff, H.K. Heo, S. Ahn, T. Asawa, A.  
964 Murakami, H.G. Kim, A multilayer mean radiant temperature model for  
965 pedestrians in a street canyon with trees, *Build. Environ.* 141 (2018) 298–309.  
966 <https://doi.org/10.1016/j.buildenv.2018.05.058>.

- 967 [34] C.Y. Park, D.K. Lee, E.S. Krayenhoff, H.K. Heo, J.H. Hyun, K. Oh, T.Y. Park,  
968 Variations in pedestrian mean radiant temperature based on the spacing and size  
969 of street trees, *Sustain. Cities Soc.* 48 (2019) 1–9.  
970 <https://doi.org/10.1016/j.scs.2019.101521>.
- 971 [35] T. Zölch, J. Maderspacher, C. Wamsler, S. Pauleit, Using green infrastructure for  
972 urban climate-proofing: An evaluation of heat mitigation measures at the micro-  
973 scale, *Urban For. Urban Green.* 20 (2016) 305–316.  
974 <https://doi.org/10.1016/j.ufug.2016.09.011>.
- 975 [36] T.E. Morakinyo, K.K.L. Lau, C. Ren, E. Ng, Performance of Hong Kong’s  
976 common trees species for outdoor temperature regulation, thermal comfort and  
977 energy saving, *Build. Environ.* 137 (2018) 157–170.  
978 <https://doi.org/10.1016/j.buildenv.2018.04.012>.
- 979 [37] D. Armson, M.A. Rahman, A.R. Ennos, A comparison of the shading  
980 effectiveness of five different street tree species in Manchester, UK, *Arboric.*  
981 *Urban For.* 39 (2013) 157–164.
- 982 [38] M.A. Rahman, D. Armson, A.R. Ennos, A comparison of the growth and cooling  
983 effectiveness of five commonly planted urban tree species, *Urban Ecosyst.* 18  
984 (2015) 371–389. <https://doi.org/10.1007/s11252-014-0407-7>.
- 985 [39] L. Zhang, Q. Zhan, Y. Lan, Effects of the tree distribution and species on outdoor  
986 environment conditions in a hot summer and cold winter zone: A case study in  
987 Wuhan residential quarters, *Build. Environ.* 130 (2018) 27–39.  
988 <https://doi.org/10.1016/j.buildenv.2017.12.014>.

- 989 [40] R. Sanusi, D. Johnstone, P. May, S.J. Livesley, Microclimate benefits that  
990 different street tree species provide to sidewalk pedestrians relate to differences  
991 in Plant Area Index, *Landsc. Urban Plan.* 157 (2017) 502–511.  
992 <https://doi.org/10.1016/j.landurbplan.2016.08.010>.
- 993 [41] X. Chen, P. Zhao, Y. Hu, *et al.*, Canopy transpiration and its cooling effect of  
994 three urban tree species in a subtropical city- Guangzhou, China, *Urban For.*  
995 *Urban Green.* 43 (2019) 126368. <https://doi.org/10.1016/j.ufug.2019.126368>.
- 996 [42] M. Jiao, W. Zhou, Z. Zheng, *et al.*, Patch size of trees affects its cooling  
997 effectiveness: A perspective from shading and transpiration processes, *Agric. For.*  
998 *Meteorol.* 247 (2017) 293–299. <https://doi.org/10.1016/j.agrformet.2017.08.013>.
- 999 [43] E. Litvak, H.R. McCarthy, D.E. Pataki, A method for estimating transpiration of  
1000 irrigated urban trees in California, *Landsc. Urban Plan.* 158 (2017) 48–61.  
1001 <https://doi.org/10.1016/j.landurbplan.2016.09.021>.
- 1002 [44] M.A. Rahman, A. Moser, A. Gold, T. Rötzer, S. Pauleit, Vertical air temperature  
1003 gradients under the shade of two contrasting urban tree species during different  
1004 types of summer days, *Sci. Total Environ.* 633 (2018) 100–111.  
1005 <https://doi.org/10.1016/j.scitotenv.2018.03.168>.
- 1006 [45] J. Konarska, J. Uddling, B. Holmer, M. Lutz, F. Lindberg, H. Pleijel, S. Thorsson,  
1007 Transpiration of urban trees and its cooling effect in a high latitude city, *Int. J.*  
1008 *Biometeorol.* 60 (2016) 159–172. <https://doi.org/10.1007/s00484-015-1014-x>.
- 1009 [46] C. Wang, Z.H. Wang, C. Wang, S.W. Myint, Environmental cooling provided by  
1010 urban trees under extreme heat and cold waves in U.S. cities, *Remote Sens.*

- 1011 Environ. 227 (2019) 28–43. <https://doi.org/10.1016/j.rse.2019.03.024>.
- 1012 [47] M.A. Rahman, A. Moser, T. Rötzer, S. Pauleit, Comparing the transpirational  
1013 and shading effects of two contrasting urban tree species, *Urban Ecosyst.* 22  
1014 (2019) 683–697. <https://doi.org/10.1007/s11252-019-00853-x>.
- 1015 [48] W.T.L. Chow, A.J. Brazel, Assessing xeriscaping as a sustainable heat island  
1016 mitigation approach for a desert city, *Build. Environ.* 47 (2012) 170–181.  
1017 <https://doi.org/10.1016/j.buildenv.2011.07.027>.
- 1018 [49] A. Middel, N. Chhetri, R. Quay, Urban forestry and cool roofs: Assessment of  
1019 heat mitigation strategies in Phoenix residential neighborhoods, *Urban For.*  
1020 *Urban Green.* 14 (2015) 178–186. <https://doi.org/10.1016/j.ufug.2014.09.010>.
- 1021 [50] C.Y. Park, D.K. Lee, E.S. Krayenhoff, *et al.*, Variations in pedestrian mean  
1022 radiant temperature based on the spacing and size of street trees, *Sustain. Cities*  
1023 *Soc.* (2019). <https://doi.org/10.1016/j.scs.2019.101521>.
- 1024 [51] L.V. de Abreu-Harbich, L.C. Labaki, A. Matzarakis, Effect of tree planting  
1025 design and tree species on human thermal comfort in the tropics, *Landsc. Urban*  
1026 *Plan.* 138 (2015) 99–109. <https://doi.org/10.1016/j.landurbplan.2015.02.008>.
- 1027 [52] Z. Tan, K.K.L. Lau, E. Ng, Planning strategies for roadside tree planting and  
1028 outdoor comfort enhancement in subtropical high-density urban areas, *Build.*  
1029 *Environ.* 120 (2017) 93–109. <https://doi.org/10.1016/j.buildenv.2017.05.017>.
- 1030 [53] Z. Wu, L. Chen, Optimizing the spatial arrangement of trees in residential  
1031 neighborhoods for better cooling effects: Integrating modeling with in-situ  
1032 measurements, *Landsc. Urban Plan.* 167 (2017) 463–472.

- 1033 <https://doi.org/10.1016/j.landurbplan.2017.07.015>.
- 1034 [54] Z. Wu, P. Dou, L. Chen, Comparative and combinative cooling effects of  
1035 different spatial arrangements of buildings and trees on microclimate, *Sustain.*  
1036 *Cities Soc.* (2019). <https://doi.org/10.1016/j.scs.2019.101711>.
- 1037 [55] Q. Zhao, D.J. Sailor, E.A. Wentz, Impact of tree locations and arrangements on  
1038 outdoor microclimates and human thermal comfort in an urban residential  
1039 environment, *Urban For. Urban Green.* 32 (2018) 81–91.  
1040 <https://doi.org/10.1016/j.ufug.2018.03.022>.
- 1041 [56] M. Aminipouri, D. Rayner, F. Lindberg, *et al.*, Urban tree planting to maintain  
1042 outdoor thermal comfort under climate change: The case of Vancouver’s local  
1043 climate zones, *Build. Environ.* 158 (2019) 226–236.  
1044 <https://doi.org/10.1016/j.buildenv.2019.05.022>.
- 1045 [57] Z.H. Wang, Monte Carlo simulations of radiative heat exchange in a street  
1046 canyon with trees, *Sol. Energy.* 110 (2014) 704–713.  
1047 <https://doi.org/10.1016/j.solener.2014.10.012>.
- 1048 [58] T.E. Morakinyo, Y.F. Lam, Simulation study on the impact of tree-configuration,  
1049 planting pattern and wind condition on street-canyon’s micro-climate and  
1050 thermal comfort, *Build. Environ.* 103 (2016) 262–275.  
1051 <https://doi.org/10.1016/j.buildenv.2016.04.025>.
- 1052 [59] T. Eckmann, A. Morach, M. Hamilton, *et al.*, A. McNamee, A. Haripriyan, D.  
1053 Castillo, S. Grandy, A. Kessi, Measuring and modeling microclimate impacts of  
1054 *Sequoiadendron giganteum*, *Sustain. Cities Soc.* 38 (2018) 509–525.

- 1055 <https://doi.org/10.1016/j.scs.2017.12.028>.
- 1056 [60] S.H. Lee, S.U. Park, A vegetated urban canopy model for meteorological and  
1057 environmental modelling, *Boundary-Layer Meteorol.* 126 (2008) 73–102.  
1058 <https://doi.org/10.1007/s10546-007-9221-6>.
- 1059 [61] H. Simon, J. Lindén, D. Hoffmann, P. Braun, M. Bruse, J. Esper, Modeling  
1060 transpiration and leaf temperature of urban trees – A case study evaluating the  
1061 microclimate model ENVI-met against measurement data, *Landsc. Urban Plan.*  
1062 174 (2018) 33–40. <https://doi.org/10.1016/j.landurbplan.2018.03.003>.
- 1063 [62] J. Deng, B.J. Pickles, A. Kavakopoulos, T. Blanus, C.H. Halios, S.T. Smith, L.  
1064 Shao, Concept and methodology of characterising infrared radiative  
1065 performance of urban trees using tree crown spectroscopy, *Build. Environ.* 157  
1066 (2019) 380–390. <https://doi.org/10.1016/j.buildenv.2019.04.056>.
- 1067 [63] British Trees: native and non-native trees.  
1068 [https://www.woodlandtrust.org.uk/visiting-woods/trees-woods-and-](https://www.woodlandtrust.org.uk/visiting-woods/trees-woods-and-wildlife/british-trees/)  
1069 [wildlife/british-trees/](https://www.woodlandtrust.org.uk/visiting-woods/trees-woods-and-wildlife/british-trees/) (accessed June 21, 2019).
- 1070 [64] C.F. Dietrich, *Uncertainty, calibration and probability: The statistics of scientific*  
1071 *and industrial measurement*, 2nd ed., New York, 1991.  
1072 <https://doi.org/10.1201/9780203734759>.
- 1073 [65] R Core Team, *R: A language and environment for statistical computing*, (2019).  
1074 <https://www.r-project.org/>.
- 1075 [66] W.H. Oksanen J, Blanchet FG, Friendly M, et al., *vegan: Community Ecology*  
1076 *Package. R package version 2.5-6*, (2019). <https://cran.r->

1077 project.org/package=vegan.

1078 [67] M.F. Kassambara A, factoextra: Extract and Visualize the Results of Multivariate  
1079 Data Analyses, (2017). <https://cran.r-project.org/package=factoextra>.

1080 [68] S. Lê, J. Josse, F. Husson, FactoMineR: An R package for multivariate analysis,  
1081 J. Stat. Softw. 25 (2008) 1–18. <https://doi.org/10.18637/jss.v025.i01>.

1082 [69] P. Legendre, L. Legendre, Numerical Ecology, 3rd Editio, Elsevier, Amsterdam,  
1083 Netherlands, 2012. [https://www.elsevier.com/books/numerical-](https://www.elsevier.com/books/numerical-ecology/legendre/978-0-444-53868-0)  
1084 [ecology/legendre/978-0-444-53868-0](https://www.elsevier.com/books/numerical-ecology/legendre/978-0-444-53868-0).

1085 [70] J. Cavender-Bares, J.E. Meireles, J.J. Couture, *et al.*, Associations of leaf spectra  
1086 with genetic and phylogenetic variation in oaks: Prospects for remote detection  
1087 of biodiversity, Remote Sens. 8 (2016). <https://doi.org/10.3390/rs8030221>.

1088 [71] ImageJ User Guide. <https://imagej.nih.gov/ij/docs/guide/index.html> (accessed  
1089 September 20, 2019).

1090 [72] Reading, ENG, United Kingdom — Sunrise, Sunset, and Moon Times.  
1091 <https://www.timeanddate.com/astronomy/uk/reading> (accessed June 10, 2019).

1092 [73] Horse chestnut leaf-mining moth. <https://www.rhs.org.uk/advice/profile?pid=533>  
1093 (accessed September 8, 2019).

1094 [74] D.S. Falster, M. Westoby, Leaf size and angle vary widely across species: What  
1095 consequences for light interception?, New Phytol. 158 (2003) 509–525.  
1096 <https://doi.org/10.1046/j.1469-8137.2003.00765.x>.